PLOS | ONE

Interaction between Nbp35 and Cfd1 Proteins of Cytosolic Fe-S Cluster Assembly Reveals a Stable Complex Formation in *Entamoeba histolytica*

Shadab Anwar[1], Manas Ranjan Dikhit[2], Krishn Pratap Singh[1], Rajiv Kumar Kar[2], Amir Zaidi[1], Ganesh Chandra Sahoo[2], Awadh Kishore Roy[3], Tomoyoshi Nozaki[4], Pradeep Das[5], Vahab Ali[1]*

1 Laboratory of Molecular Biochemistry and Cell Biology, Department of Biochemistry, Rajendra Memorial Research Institute of Medical Sciences, Agam-kuan, Patna, India, **2** Department of Biomedical Informatics Centre, Rajendra Memorial Research Institute of Medical Sciences, Agam-kuan, Patna, India, **3** Department of Botany, T. M. Bhagalpur University, Bhagalpur, India, **4** Department of Parasitology, National Institute of Infectious Diseases, Shinjuku-ku, Tokyo, Japan, **5** Department of Molecular Biology, Rajendra Memorial Research Institute of Medical Sciences, Agam-kuan, Patna, India

Abstract

Iron-Sulfur (Fe-S) proteins are involved in many biological functions such as electron transport, photosynthesis, regulation of gene expression and enzymatic activities. Biosynthesis and transfer of Fe-S clusters depend on Fe-S clusters assembly processes such as ISC, SUF, NIF, and CIA systems. Unlike other eukaryotes which possess ISC and CIA systems, amitochondriate *Entamoeba histolytica* has retained NIF & CIA systems for Fe-S cluster assembly in the cytosol. In the present study, we have elucidated interaction between two proteins of *E. histolytica* CIA system, Cytosolic Fe-S cluster deficient 1 (Cfd1) protein and Nucleotide binding protein 35 (Nbp35). *In-silico* analysis showed that structural regions ranging from amino acid residues (P33-K35, G131-V135 and I147-E151) of Nbp35 and (G5-V6, M34-D39 and G46-A52) of Cfd1 are involved in the formation of protein-protein complex. Furthermore, Molecular dynamic (MD) simulations study suggested that hydrophobic forces surpass over hydrophilic forces between Nbp35 and Cfd1 and Van-der-Waal interaction plays crucial role in the formation of stable complex. Both proteins were separately cloned, expressed as recombinant fusion proteins in *E. coli* and purified to homogeneity by affinity column chromatography. Physical interaction between Nbp35 and Cfd1 proteins was confirmed *in vitro* by co-purification of recombinant Nbp35 with thrombin digested Cfd1 and *in vivo* by pull down assay and immunoprecipitation. The *insilico, in vitro* as well as *in vivo* results prove a stable interaction between these two proteins, supporting the possibility of its involvement in Fe-S cluster transfer to target apo-proteins through CIA machinery in *E. histolytica*. Our study indicates that initial synthesis of a Fe-S precursor in mitochondria is not necessary for the formation of Cfd1-Nbp35 complex. Thus, Cfd1 and Nbp35 with the help of cytosolic NifS and NifU proteins can participate in the maturation of non-mitosomal Fe-S proteins without any apparent assistance of mitosomes.

Citation: Anwar S, Dikhit MR, Singh KP, Kar RK, Zaidi A, et al. (2014) Interaction between Nbp35 and Cfd1 Proteins of Cytosolic Fe-S Cluster Assembly Reveals a Stable Complex Formation in *Entamoeba histolytica*. PLoS ONE 9(10): e108971. doi:10.1371/journal.pone.0108971

Editor: Tracey Rouault, National Institute of Child Health and Human Development, United States of America

Received March 8, 2014; **Accepted** August 29, 2014; **Published** October 1, 2014

Data Availability: The authors confirm that all data underlying the findings are fully available without restriction. All data are included within the paper.

Funding: This work was supported by a grant from Indian Council of Medical Research (ICMR), Ministry of Health and Family Welfare, and Department of Science & Technology (DST/INT/JSPSP-117), New Delhi, India. The funder had no role in study design, data collection and analysis decision to publish, or preparation of the manuscript.

Competing Interests: The authors have declared that no competing interests exist.

* Email: vahab_ali@yahoo.com

Introduction

Entamoeba histolytica is one of the most widespread and clinically important protozoan parasite causing both intestinal (amoebic colitis) and extra intestinal (amoebic liver abscess) disease throughout the world, resulting to an estimated 40,000 to 110,000 deaths annually. World Health Organisation estimate (WHO, 1998) places *E. histolytica* second after *Plasmodium falciparum* in causing abundant annual death among protozoan parasites. *E. histolytica* lacks a defined structure of mitochondria and its functions [1]. However, mitochondrion residual organelle known as mitosome [2] is present in this parasite. Mitochondria performs many crucial roles in various biochemical and iron-requiring biosynthetic processes; namely, heme formation, Iron-Sulfur (Fe-S) clusters biogenesis and cellular iron regulation [3,4]. Among them, Iron-Sulfur clusters biogenesis is essential for the maturation of Fe-S proteins which are biologically functional and ubiquitous components that orchestrate a wide range of biochemical machinery and efficiently regulate the metabolic cascades in living organisms for sustainable and fundamental life processes [4–8]. Mitochondria assemble Fe-S clusters for their own set of mitochondrial Fe-S proteins as well as crucially involved in the biogenesis and maturation of Fe-S proteins located in the cytosol and nucleus [9–11].

Despite the chemical simplicity of Fe-S clusters, Fe-S clusters biogenesis is a complex process involving three types of systems, viz, Iron Sulfur Clusters (ISC), Sulfur Utilization Factors (SUF) and Nitrogen Fixation (NIF) systems. The ISC system is a house-keeping system involving ~30 protein components [8,12–14] and among them 10 proteins have been conserved from bacteria to human [15,16]. The majority of protozoan parasites have retained

ISC system either in mitochondrion or mitochondria like organelles; mitosomes, hydrogenosomes, and mitochondria related organelles (MROs) [17–20]. However, *Plasmodium spp.* & *Blastocystis hominis* possess SUF system or some of its components in addition to the canonical ISC system which is functional under oxidative stress and iron deficient conditions [19,21–23]. Nitrogen-fixation (NIF) system is present in nitrogen fixing bacteria, cyanobacteria and microaerophilic bacteria but absent in eukaryotes and protozoan parasites except *E. histolytica* and free living amoeba (*Mastigamoeba balamuthi*). Thus, Fe-S cluster biogenesis in *E. histolytica* solely depends on NIF system [24]. It has already been proved that the NIF system alone is required for the biosynthesis of Fe-S cluster in *E. histolytica* under anaerobic conditions [24]. This organism possesses two components of NIF machinery: NifS and NifU [24,25] that are responsible for Fe-S cluster assembly. Surprisingly, *M. balamuthi* possesses two types of NifS and NifU components, of which one of them has retained targeting signal and localized in the mitosomes [26]. Contrary to the mitosomes of *M. balamuthi*, *E. histolytica* mitosomes have no evidence of classic Fe-S cluster machinery. Therefore, cytosolic NIF machinery predominantly regulates the cellular requirements for Fe-S cluster biogenesis in this organism. *E. histolytica* possess mitosomes that do not generate ATP unlike other protozoan parasites harbouring MROs (*Blastocystis sp.*) or hydrogenosomes which are involved in both ATP generation and Fe-S cluster biogenesis [27]. However, neither amoebic mitosomes possesses the ISC machinery, nor any component of ISC or SUF machinery has been identified in *E. histolytica* genome [23]. It has not been resolved till-date how NIF system works in connection with Cytosolic Iron-sulfur protein Assembly (CIA) in the absence of true mitochondria. It also remains unknown whether NIF and CIA system interact with each other for biogenesis and subsequent transfer of Fe-S clusters to apoproteins, as both systems co-exist in the cytoplasm.

In eukaryotes, the ISC system assists for the maturation of cytosolic/nuclear Fe-S proteins including CIA machinery components. The CIA system is limited to cytoplasm and core protein assembly consists of Cfd1, Nbp35, Nar1, Cia1, Dre2, Tah18 [28–34] and some additional components (MMS19, MIP18 and ANT2) which are exclusively present in mammalian system [35]. MMS19 function as part of the CIA machinery which interacts and facilitate Fe-S cluster targeting to apo-proteins involved in methionine biosynthesis, DNA replication, DNA repair, and telomerase maintenance [36]. In addition, MMS19 forms a complex with CIA proteins (CIAO1, IOP1, & MIP18) involved in DNA metabolism and its presence is necessary for DNA replication and repair [37]. The CIA1 (CIAO1) associates with either CIA2A (FAM96A) or CIA2B (FAM96B) and MMS19 proteins. It has been reported recently that CIA2B-CIA1-MMS19 complex binds to and facilitates assembly of most cytosolic/nuclear Fe-S proteins but CIA2A is specially required for the maturation of iron regulatory protein 1 (IRP1), which is involved in cellular iron homeostasis [38]. The CIA2A is also involved in stabilization of IRP2 through its interaction with IRP2. However, *E. histolytica*, comprised of a NIF system has also retained CIA components namely; Cfd1, Nbp35, Nar1, Dre2, and Cia1 [23]. Cfd1 and Nbp35 belong to a subfamily of deviant P-loop NTPases, often referred to as the MRP/NBP35 sub-family, which appear to function in Fe-S clusters biogenesis in all kingdoms. The first component of the CIA machinery to be identified was Cfd1 which is an essential and highly conserved P-loop NTPase [29]. *In vitro* reconstitution study has shown that Nbp35 forms an oligomeric complex with Cfd1 and both can assemble labile Fe-S cluster on their conserved cysteine residues of C- terminal domain. They may serve as transient scaffold for Fe-S cluster before transfer to apo-proteins in yeast [39,40]. The class of NTPases typically form homodimer involving a signature lysine (Lys26 in Cfd1 and Lys81 in Nbp35) residue within the walker A (Nucleotide binding) motif which also plays a role in ATP binding

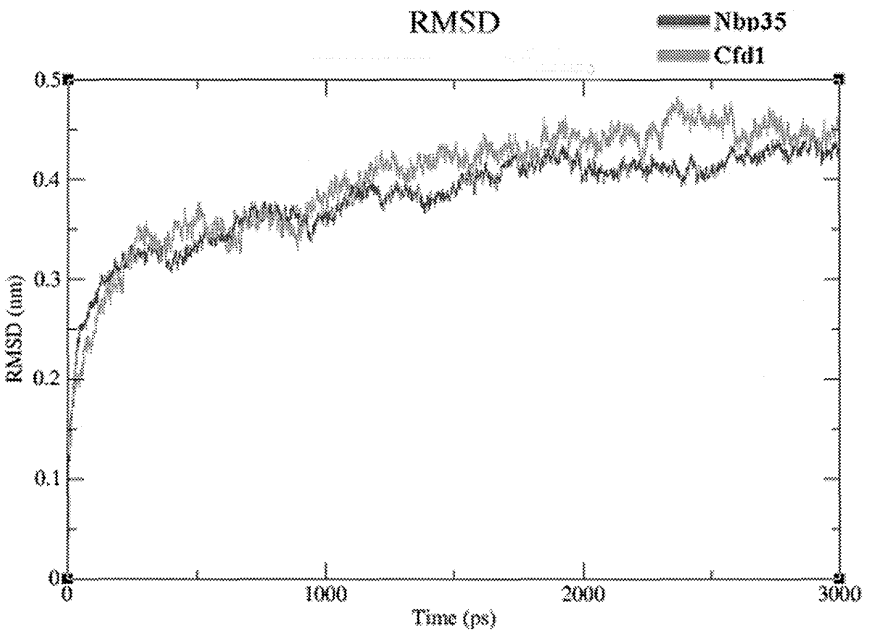

Figure 1. RMSDs time scan for Nbp35 and Cfd1. Backbone RMSDs are shown as a function of time for Nbp35 (red) and Cfd1 (green) protein at 3 ns.
doi:10.1371/journal.pone.0108971.g001

and/or hydrolysis [41]. However, in plantae including *Arabidopsis thaliana*, Cfd1 is absent and Npb35 works alone as the scaffold component [42,43]. Although, Cfd1 gene is absent in some organisms such as *Caenorhabditis elegans* (metazoa) and plantae [43]; the specific functional role of Cfd1 is its interaction with Nbp35 which alters the character of Nbp35-bound Fe-S clusters, making it more labile and enhancing transfer to apo-target Fe-S proteins [41].

In the present study, we have attempted to investigate the interaction between Cfd1 and Nbp35 in *E. histolytica in vivo* by co-purification and immunoprecipitation and *insilico* using molecular dynamics simulation tool. Our results show that Npb35 and Cfd1 of *E. histolytica* interacts with each other to form a stable complex and each protein has the potential to coordinate a 4Fe-4S cluster on it similar to the earlier report in yeast [30,40]. This would be the first report showing interaction and stable complex formation between two components of CIA machinery Nbp35 and Cfd1 in an amitochondriate protozoan parasite possessing a cytosolic NIF system for Fe-S cluster assembly.

Materials and Methods

Chemicals and reagents

All chemicals of analytical grade were purchased and used from Sigma-Aldrich, Amresco (USA), Merck, and USB (USA) unless otherwise stated. Chromatography column was purchased from Bio-Rad. Ni^{+2}-NTA agarose was purchased from Qiagen. Adult bovine serum from Hyclone, Yeast extract and Casitone were purchased from BD Biosciences.

Microorganism and cultivation

E. histolytica trophozoites clonal strain (HM-1: IMMS cl 6) was maintained axenically in TYIS-33 medium supplemented with 15% adult bovine serum at 35.5°C [44]. Trophozoites were harvested in the late-logarithmic growth phase 2–3 days after the inoculation of medium with one- thirtieth to one-twelfth of the total culture volume. After the cultures were chilled on ice for 5 mins, trophozoites were collected by centrifugation at 500×g for 10 mins at 4°C and washed twice with ice-cold phosphate-

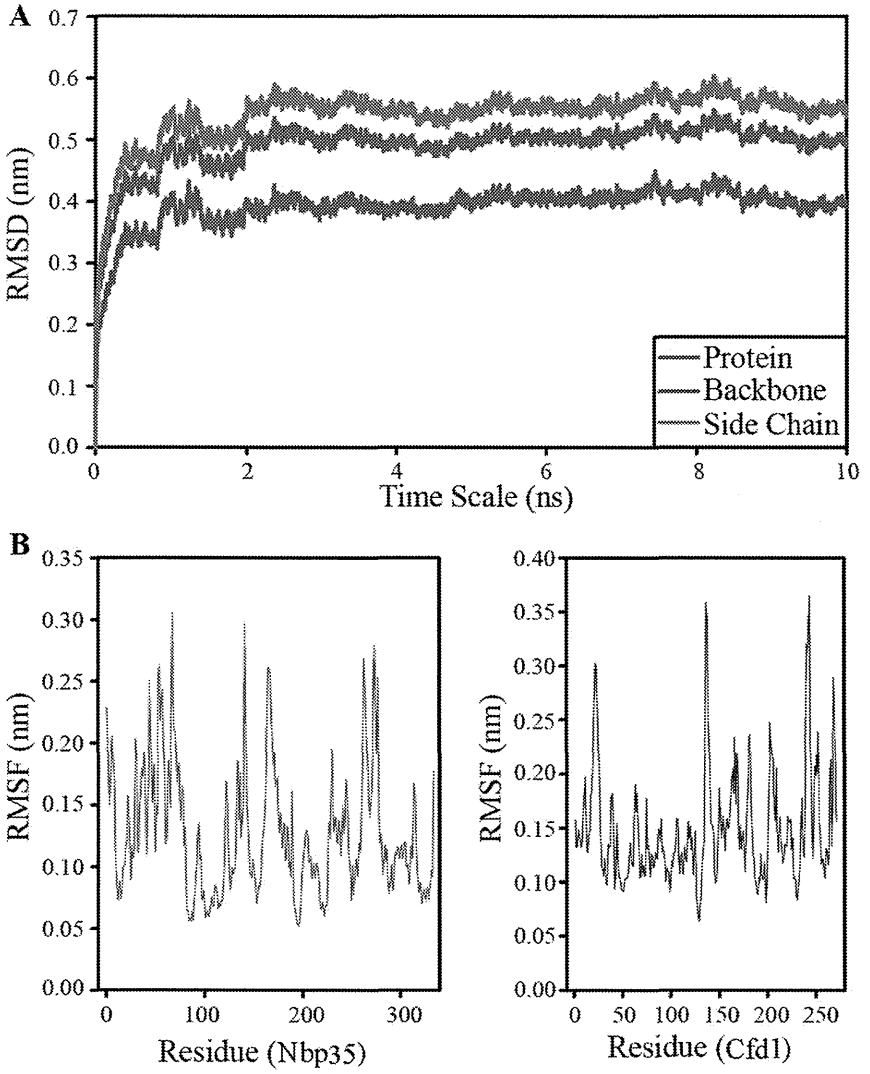

Figure 2. RMSD and RMSF profile of Nbp35-Cfd1 complex. (A) RMSD profile of Nbp35-Cfd1 complex for all-atoms (red), backbone atoms (blue) and side chain (green) plotted as a function of time (B) Root mean square fluctuation for Nbp35 and Cfd1 plotted against time from MD simulation.
doi:10.1371/journal.pone.0108971.g002

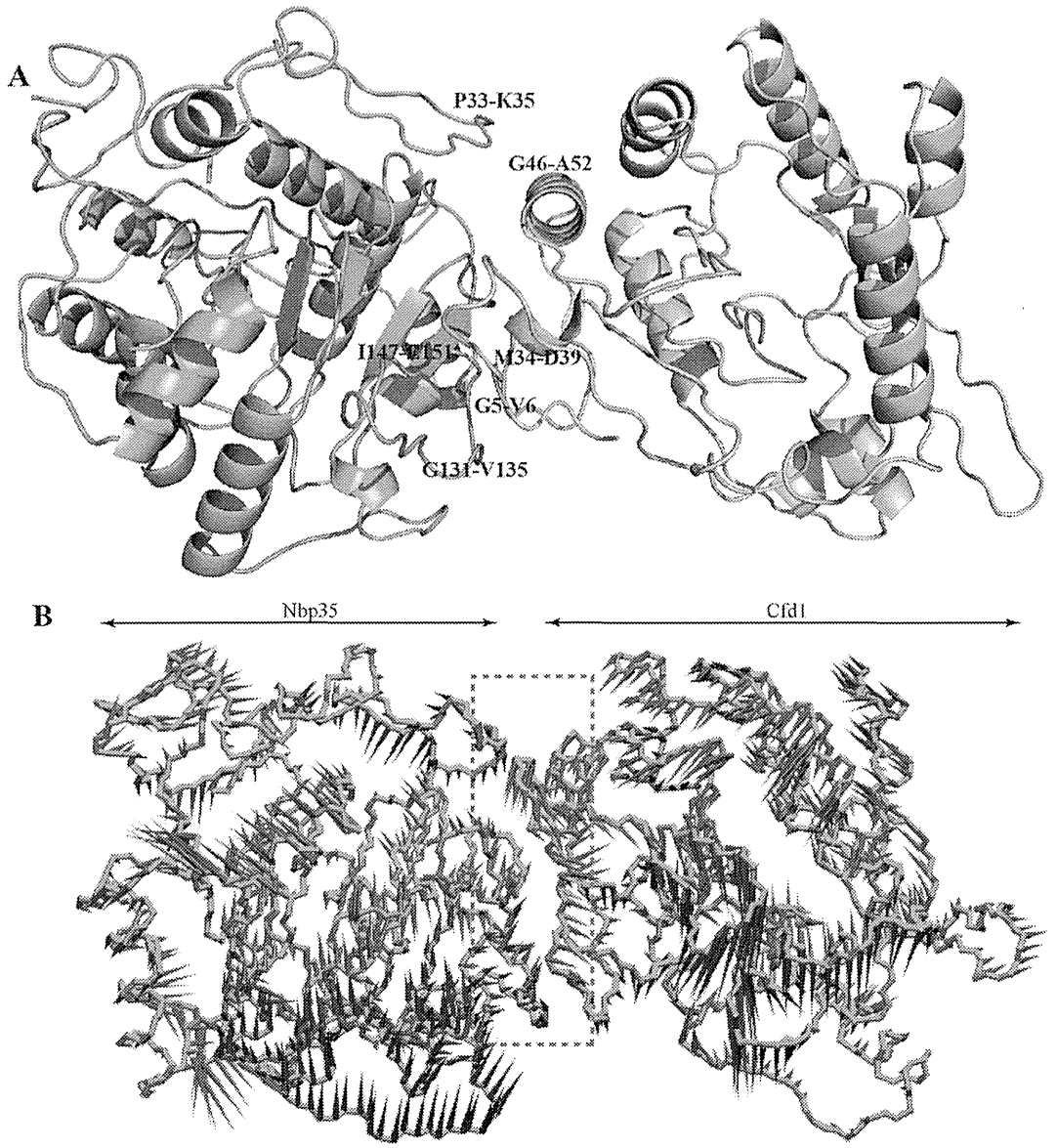

Figure 3. Nbp35-Cfd1 complex structure showing the regions involved in interaction. (A) Complex structure of Nbp35-Cfd1 where the molecular contacts are highlighted (blue–Nbp35) and (green-Cfd1) with mentioned residues involved in interaction. (B) Porcupine plots for Nbp35-Cfd1 complex showing backbone fluctuation from simulation time course. The regions involved in contact are highlighted with dotted region.
doi:10.1371/journal.pone.0108971.g003

buffered saline (PBS), pH 7.4 [45]. Cell pellets were stored at −30°C until use.

PCR amplification and cloning of Nbp35 & Cfd1 genes

Based on the nucleotide sequence of the protein-encoding region of the putative *E. histolytica* Nucleotide binding proteins genes (*Nbp35,* accession number XP_650593, EHI_047750; Cfd1 accession number XP_653192; EHI_000610); primers (shown below) were designed to clone Nbp35 & Cfd1 in vector pET15b with a histidine tag at the amino terminus. The *Nbp35 & Cfd1* ORFs were amplified from cDNA of *E. histolytica* with a sense (5′CCT**CAT*ATG***AGTTGTTCTCATAATTGTTCA-3′) and an antisense (5′-CCA**GGATCC***TTA*AAGATTTGTTATTATTT-CCTT-3′) primers for Nbp35 and a sense (5′CCT**CAT*ATG***ACT-GAACTTAACTCTGATCGT-3′) and an antisense (5′-CCA**G-GATCC***TTA*AGCAAAAGTTTTAGCAAGATCG-3′) primers for Cfd1, where *Nde*I and *Bam*HI-sites are underlined and the translation initiation and termination codons are italicized. PCR was performed in a 50 µl volume containing 0.25 mM each dNTPs, 2.0 mM $MgCl_2$ 1.0 µM each primer, 1 µg cDNA (*E. histolytica*) and 1.0 U Pfu DNA polymerase. The conditions used to amplify the *Nbp35 & Cfd1* genes were hot start at 94°C for 5 mins, denaturation at 94°C for 30 s, annealing at 55°C for 30 s, elongation at 68°C for 1.0 min and subjected to 30 cycles with a final extension for 10 mins at 68°C. A ~1.0 & 0.8 kb PCR products were observed on 1.0% agarose gel electrophoresis. These PCR products were double digested with *Nde*I and *Bam*HI, electrophoresed, purified with gel extraction kit (Qiagen), and cloned into *Nde*I and *Bam*HI- digested pET-15b (Novagen) in the same orientation as the T7 promoter. The ligated mixture was transformed in competent DH5α cells (Novagen) which produced the pET-15b-Nbp35 & pET-15b-Cfd1 plasmids. The insert and

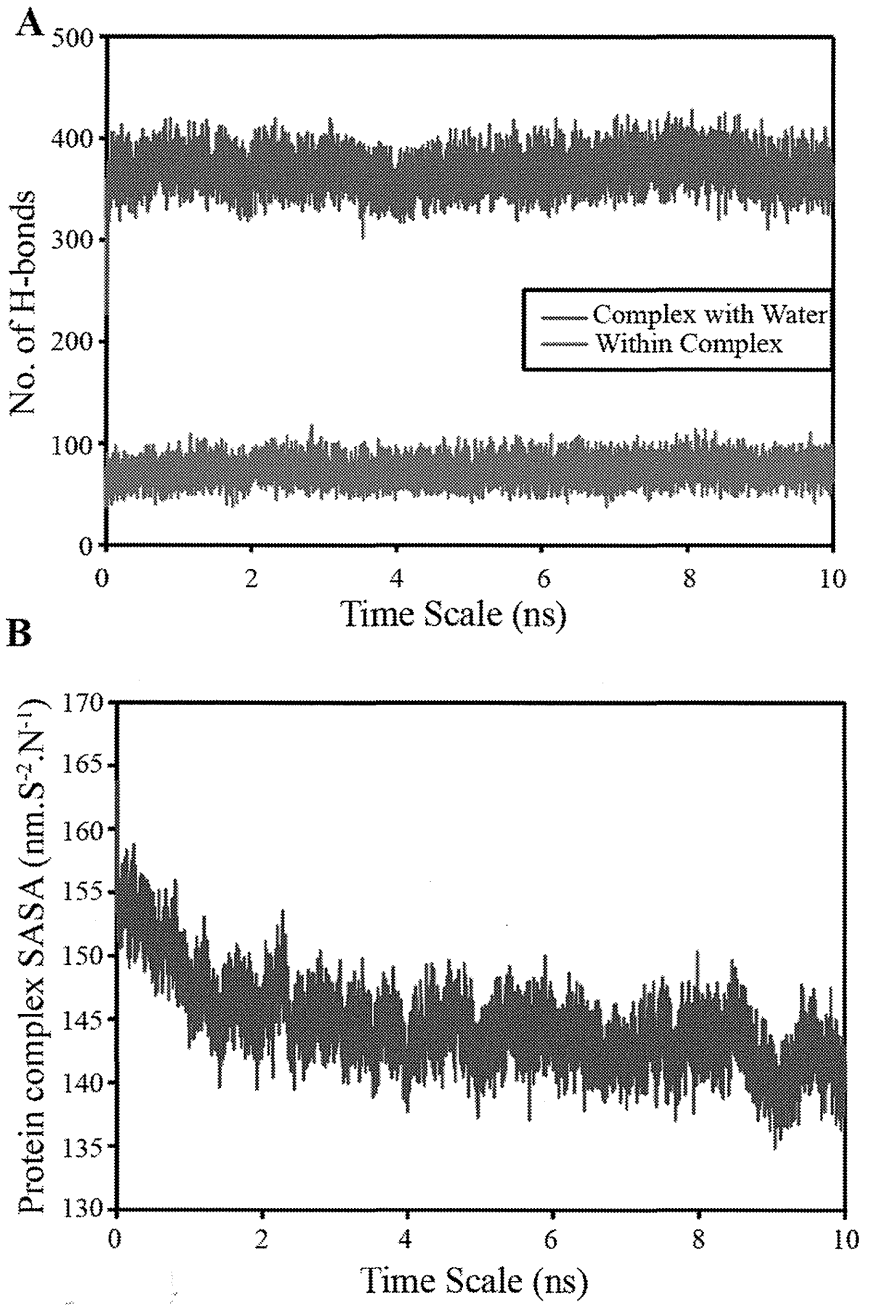

Figure 4. Hydrogen bonding profile & solvent accessibility. (A) Hydrogen bonding profile indicating numbers of hydrogen bonds formed within protein atoms and with water molecules. (B) Solvent accessible surface area computed over the simulation time course.
doi:10.1371/journal.pone.0108971.g004

ORF orientation were confirmed by colony PCR. Construct plasmids were isolated using Qiagen miniprep kit as per manufacturer's instructions. The pET-15b-Nbp35 & pET-15b-Cfd1 constructs were transformed into competent *E. coli* BL21 (DE3) (Novagen) cells by heat shock at 42°C for 45 s, and the cells were grown at 37°C on Luria Bertani (LB) agar medium in the presence of 50 μg/ml ampicillin (Amp).

Expression and purification of recombinant Nbp35 and Cfd1 Proteins

The pET-Nbp35 and pET-Cfd1 expression constructs were introduced into competent cells and the resulting single colony picked up from LB-agar plate were grown at 37°C in 5 ml of LB medium in the presence of 50 μg/ml ampicillin. The overnight culture was used to inoculate 500 ml of fresh medium and cultured at 37°C with shaking at 200 rpm. When the A_{600} reached 0.6, 0.4 mM of isopropyl β-D- thiogalactopyranoside was added to induce protein expression for 12 h at 25°C. *E. coli* cells were harvested by centrifugation at 5000 rpm for 10 mins at 4°C, the resulting cell pellet washed with PBS (pH 7.4) and resuspended in 25 ml lysis buffer [46] containing 100 μg/ml lysozyme and 1 mM Phenylmethylsulfonyl fluoride (PMSF). After 45 mins of incubation at 30°C, the cells were sonicated on ice and centrifuged at 13000 rpm for 20 mins at 4°C. The supernatant was mixed with

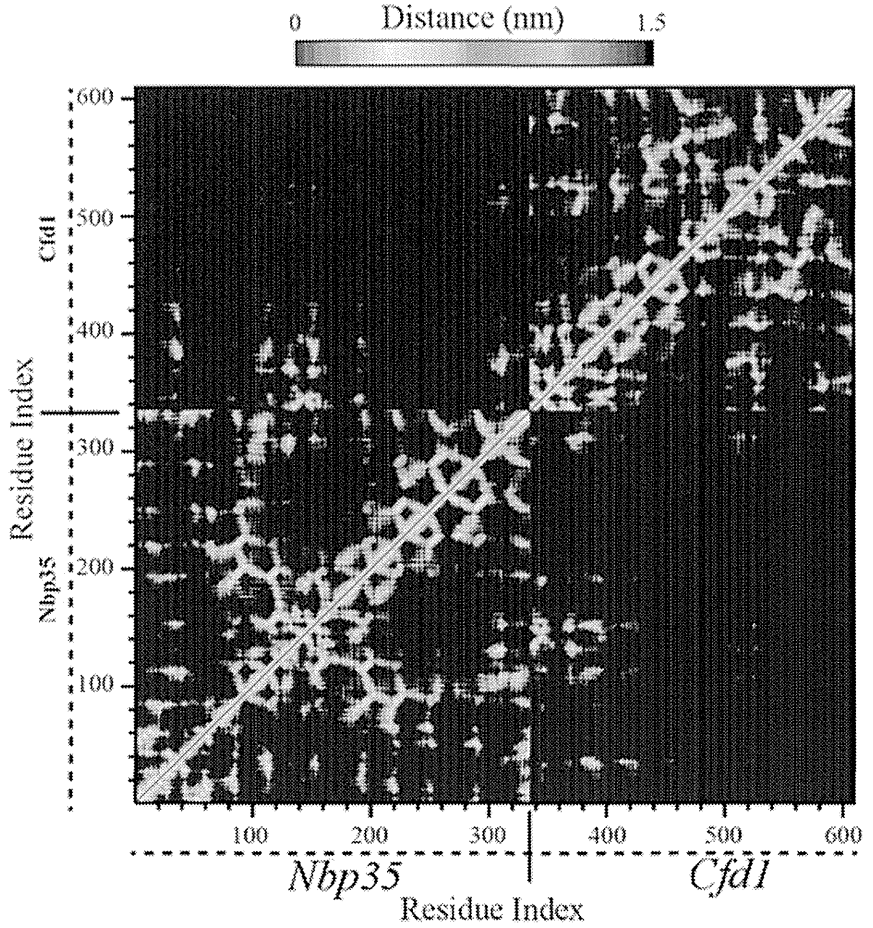

Figure 5. Contact map of Nbp35-Cfd1 complex. The contact map of Nbp35-Cfd1 complex is indicating the cross residue region involved in contact of these two proteins.
doi:10.1371/journal.pone.0108971.g005

500 µl of Ni^{+2}-NTA His-tag slurry (Qiagen) and incubated for 1.0 hr at 4°C with gentle shaking. The recombinant Nbp35 and Cfd1 protein bound resin was washed with 8–10 column volumes of buffer A (50 mM Tris-HCl, pH 8.0, 300 mM NaCl, and 0.1% Triton X-100, v/v) containing 10–50 mM of imidazole and bound proteins were eluted in 2–3 ml with buffer A containing 100–300 mM imidazole. The quality and purity of the rNbp35 and rCfd1 proteins were confirmed by 12% SDS-PAGE analysis. The proteins were extensively dialyzed against a 300 fold volume of 50 mM Tris-HCl, 150 mM NaCl, pH 8.0, containing 10% glycerol (V/V) and the complete Mini protease inhibitor cocktail (Calbiochem). The concentration of the dialyzed proteins was determined by Bradford method using bovine serum albumin as standard (U3900, Hitachi, Japan). The rNbp35 and rCfd1 proteins were stored at −30°C in 10% glycerol in small aliquots until used.

Chemical reconstitution of the Fe-S cluster on Cfd1 and Nbp35

The purified Nbp35 and Cfd1 proteins were dialyzed in 50 mM Tris-HCl, 150 mM NaCl, pH 8.0 to remove glycerol and rechecked their integrity and purity. Chemical reconstitution of Fe-S cluster on Nbp35 and Cfd1 was performed as described previously with some modifications [40–42]. Briefly, Nbp35 and Cfd1 (100 µM each protein) were reduced in reconstitution buffer (50 mM Tris-HCl, pH 8.0, 150 mM NaCl, 10 mM DTT) for 1 h at 25°C. Fresh anaerobic stocks solution of ferric ammonium citrate and Li_2S were prepared in water containing10 mM DTT before use and reconstitution of both proteins was started by the addition of 100 µM ferric ammonium citrate and 100 µM Li_2S with stirring. To avoid precipitation, the reconstitution mixture was incubated with ferric ammonium citrate for 5 min before Li_2S was added slowly drop wise to the reaction mixture followed by incubation of 2–3 hrs at 25°C. To remove non bound iron and sulphide, reconstituted proteins were desalted by PD-10 column equilibrated with reconstitution buffer containing 2 mM DTT. The assembly of Fe-S clusters into apo-proteins was monitored by UV-Vis spectroscopy (U3900, Hitachi, Japan).

Iron estimation

The iron content of Nbp35 and Cfd1 proteins were determined by the *O*- phenanthroline method as described previously [24,47]. Briefly, the Nbp35 and Cfd1 samples (80–100 µl) were acidified by the addition of 3–5 µl of concentrated HCl and then diluted with distilled water up to 0.2 ml. The mixtures were heated to 80°C for 10 mins and cooled down to room temperature. The reaction mixture was diluted with 0.6 ml of water, and 40 µl of 10% hydroxylamine hydrochloride, 0.2 ml of 0.1% *O*-phenanthroline

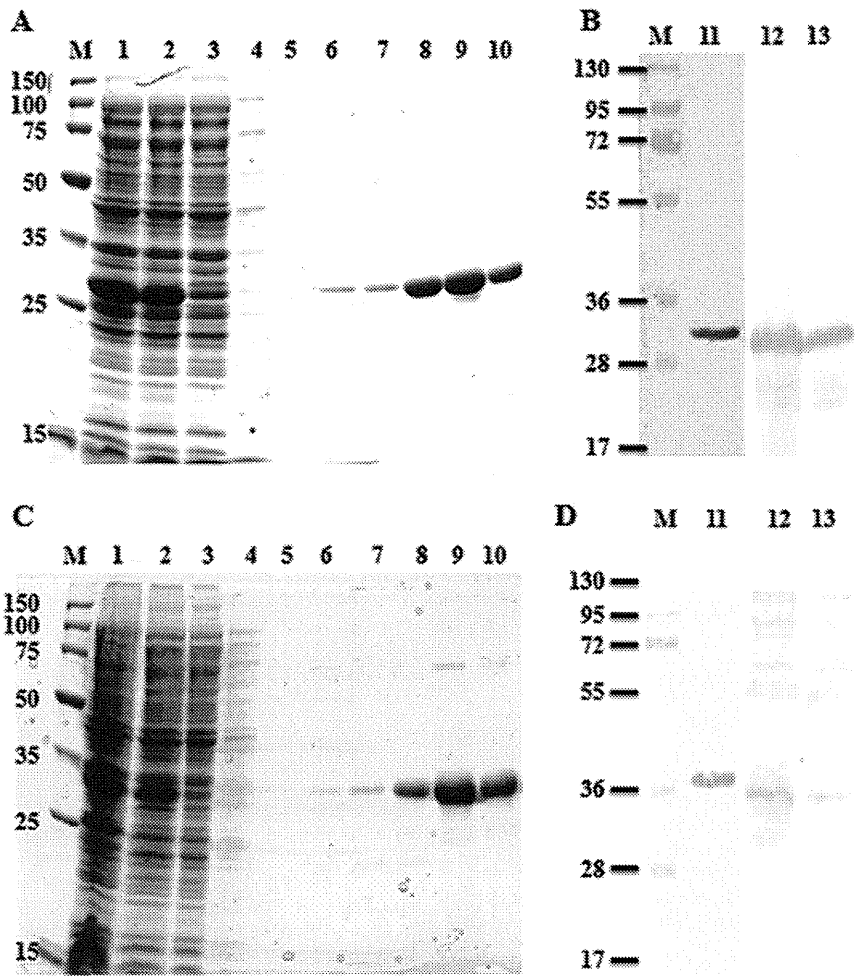

Figure 6. Purification of recombinant Cfd1 and Nbp35 protein. The recombinant Cfd1 protein was purified through Ni^{+2}-NTA column. A) Lane M-marker, lane 1-total lysate, lane 2- supernatant, lane 3-flow through, lane 4-,5-, 6-, & 7- wash (10, 20, 35, & 50 mM imidazole), lane 8- eluate (100 mM imidazole), lane 9- eluate (200 mm imidazole), lane10- eluate (300 mM imidazole). B) Immunoblot was probed with anti-Cfd1 antibody. Lane M- represents molecular weight proteins marker, lane 11- purified rCfd1 protein was probed with anti-His monoclonal antibodies, lane 12- total *E. histolytica* cell lysate, and lane-13- supernatant of *E. histolytica* lysate C) Similarly, the recombinant Nbp35 protein was purified through Ni^{+2}-NTA column Lane M-marker, lane 1- total lysate, lane 2- supernatant, lane 3- flow through, lane 4-,5-, 6-, & 7- wash (10, 20, 35, & 50 mM imidazole), lane 8- eluate (100 mM imidazole) lane 9- (200 mM imidazole), lane10- eluate (300 mM imidazole). D) Immunoblot was probed with anti-Nbp35 antibody. Lane M represents –molecular weight proteins marker, lane 11- purified rNbp35 protein was probed with anti-His monoclonal antibodies, lane 12- total *E. histolytica* cell lysate, and lane-13- supernatant of *E. histolytica* lysate.
doi:10.1371/journal.pone.0108971.g006

were added. Finally, reaction mixtures were incubated at room temperature for 30 mins, and absorbance was measured at 512 nm.

Sulfide estimation

Sulfide content of purified rNbp35 and rCfd1 proteins was determined by measuring the absorbance of a blue colour complex treated with N,N-dimethyl-p-phenylenediamine dihydrochloride (DPD) as described previously [33]. Protein samples (50 µg) were diluted up to 775 µl with water and mixed with 50 µl of 6% NaOH. The DPD reagent (0.1%) dissolved in 5 N HCl (125 µl) and 30 mM $FeCl_3$ (50 µl) solutions were added to the reaction mixture and incubated for 30 min at 30°C. Finally, reaction mixture was vortexed, centrifuged for 5 mins at 13000 rpm to remove precipitate, and absorbance of supernatant was measured at 670 nm by UV-Vis spectroscopy (U3900, Hitachi, Japan). Na_2S (0–100 µM) was used as standard.

Production of *E. histolytica* Nbp35 & Cfd1 antibodies and immunoblot analysis

Polyclonal antisera against recombinant *E. histolytica* Nbp35 or Cfd1 was raised in adult rabbit by three repeated subcutaneous injection. Pre-immune sera was collected before immunization and first dose of 300 µg Nbp35 or Cfd1 proteins emulsified in complete Freund's adjuvant was injected 8–10 places subcutaneously; followed by three booster doses of 250 µg of proteins emulsified in Freund's incomplete adjuvant. Anti-Nbp35 & Cfd1 titres were checked by ELISA after three weeks of final immunization. Finally, serum was collected from rabbits and stored at −30°C in small aliquots. Working antibodies were stored at 4°C. Prior animal ethical committee approval was taken and recommendations were strictly followed.

Cell lysate of *E. histolytica* ($\sim 1 \times 10^7$ cells/ml) was prepared using lysis buffer (100 mM Tris-HCl, pH 8.0, 300 mM NaCl, 1.0 mM EDTA, 1.0 mM DTT, 10% glycerol) as described

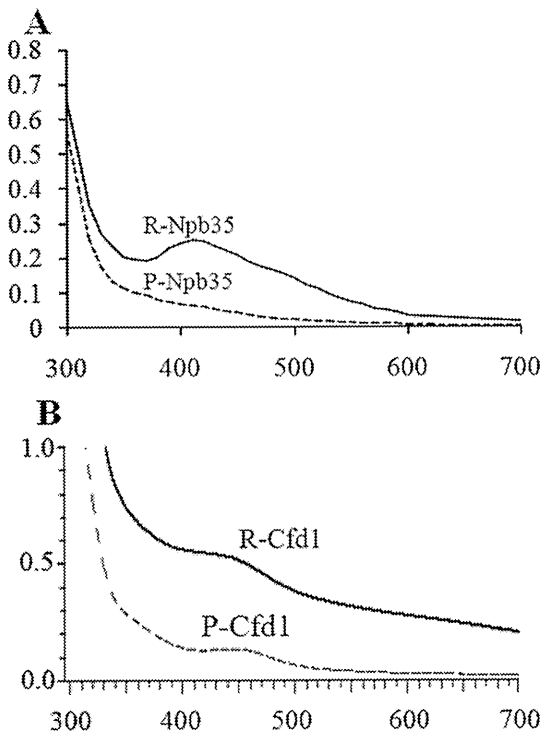

Figure 7. UV-Visible spectra of purified and reconstituted rNbp35 and rCfd1 proteins. A) As purified rNbp-35 and rNbp35 after chemical reconstitution was scanned in the UV-Vis range to detect Fe-S cluster. Solid and dashed lines represent reconstituted Nbp35 and purified Nbp35, respectively. B) UV-visible spectra of purified rCfd1 and reconstituted rCfd1protein in which, solid and dashed lines represent reconstituted rCfd1 and purified rCfd1, respectively.
doi:10.1371/journal.pone.0108971.g007

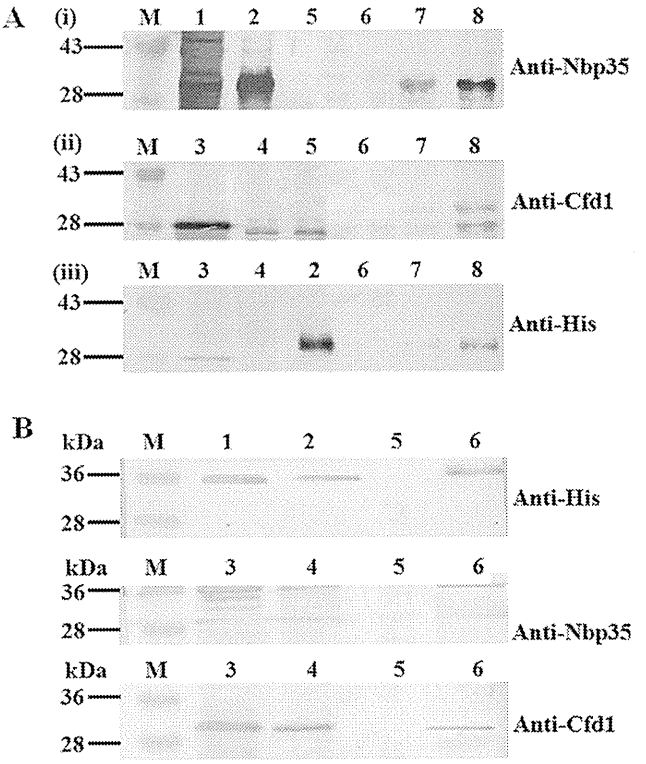

Figure 8. Interaction study between Cfd1 and Nbp35 proteins. (A) Co-purification using recombinant Nbp35 and thrombin digested Cfd1; Immunoblots of fractions obtained from co-purification experiment as described in material and methods probed with different antibodies (i) Anti-Nbp35 (ii) Anti-Cfd1 (iii) Anti-His antibodies for interaction between recombinant Nbp35 and thrombin digested Cfd1 proteins. Lane M- represents molecular weight proteins marker, lane 1- *E. coli* lysate overexpressing rNbp35, lane 2- purified rNbp35, lane 3- undigested rCfd1, lane 4- digested rCfd1, lane 5- wash (60 mM imidazole), lane 6 final wash did not show any proteins in all blots, lane 7- eluate (200 mM imidazole), lane 8- eluate (500 mM imidazole). (B) Pull down assay using rNbp35 and *E. histolytica* lysate: Ni^{+2}-NTA bound rNbp35 was incubated with *E. histolytica* lysate as described in material and methods for pull down assay and eluate (500 mM imidazole) fraction was subjected to immunoblot analysis proved different antibodies (upper panel) Anti-His (middle panel) Anti-Nbp35 (lower panel) Anti-Cfd1 antibodies for rNbp35 and endogenous amoebic Cfd1 interaction. Lane M- represents molecular weight proteins marker, lane 1- total *E. coli* lysate expressed rNbp35, lane 2- supernatant rNbp35, lane 3- total amoebic lysate, lane 4- amoebic lysate flow through, lane 5 final wash did not show any proteins in all blots, lane 6- eluate (500 mM imidazole).
doi:10.1371/journal.pone.0108971.g008

previously [24]. The protein fractions were resolved by 10% SDS-PAGE and electro-blotted on to nitrocellulose membrane. The membrane was probed with polyclonal anti-Nbp35 or Cfd1 sera (1:2000) raised in rabbit as mentioned above. ALP-conjugated goat anti-rabbit IgG (1:2000) was used as secondary antibody and blot developed with BCIP/NBT (Santa Cruz), as per manufacturer's instructions [48].

Homology modelling and Structure Validation

Prediction of an interacting complex was proceeded with homology modelling, since the crystal structures for Nbp35 and Cfd1 are not available. Full length amino acid sequences of both the proteins were retrieved from Universal Protein Resource Database (http://www.uniprot.org/). The low percentage of sequence identity in the homologues PDB structures may not fetch robust models for protein structure. Thus, we have relied upon Zhang's I-TASSER server (http://www.zhanglab.ccmb.med.umich.edu/I-TASSER/), which gives the best protein models at the Critical Assessment of Structure Prediction (CASP 7 and CASP 8), a community-wide, worldwide experiment designed to obtain an objective assessment of the state-of-the-art in structure prediction [49]. Five models of Nbp35 and Cfd1 were computationally generated using the I-TASSER algorithm. The models were selected with lowest DOPE Score and verified using the Profile 3D profile analysis method [50]. The stereo-chemical properties of both the models were investigated with Ramachandran plot using PROCHECK [51]. The quality of final model was checked using Verify-3D program [52]. In addition to this, stereo chemical qualities of 3D model were analyzed using WHATIF and ProSA web server. Molecular dyanamics (MD) simulations were conducted for the Nbp35 and Cfd1 models in explicit solvent using the GROMACS 4.0.3 (The Groningen Machine for Chemical Simulations) package. The model was solvated by water molecules in an octahedron box having edges at a distance of 0.9 nm from the molecule's periphery. The solvated system was subjected to further energy minimization to remove the steric conflicts between the atoms of protein and water molecules having a maximum step of 2000 with steepest descent integrator that converge the energy minimization when the maximum force is smaller than 1000 $kJ.mol^{-1}.nm^{-1}$. The energy minimized model was subjected to position-restrained MD with NPT ensemble keeping number of particles (N), system pressure (P) and temperature (T) as constant parameters. This was carried out for 50,000 steps for a total of

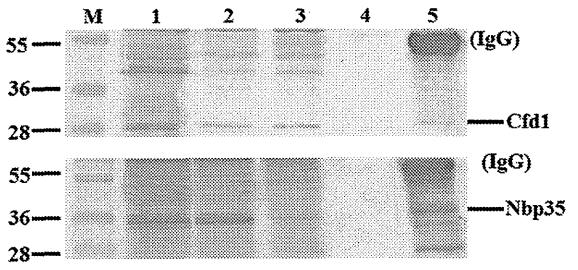

Figure 9. In-vivo interaction study Nbp35 and Cfd1 by immunoprecipitation. The anti-Nbp35 antibody bound with protein-A sepharose was incubated with amoebic lysate and immunoprecipitate was analysed by immunoblots were developed separately with anti-Cfd1 (upper panel) and anti-Nbp35 (lower panel) antibodies. IgG heavy chain (55 kda) and Cfd1 (29 Kda) were found in I.P. complex fraction and IgG heavy chain (55 kda) and Nbp35 (35 kda) bands found when probed with anti-Nbp35 antibody. Lane M- represents molecular weight proteins marker, lane 1- total amoebic lysate, lane 2- supernatant of amoebic lysate, lane 3- amoebic lysate flow through, lane 4- final wash did not show any proteins, lane 5- I.P. complex.
doi:10.1371/journal.pone.0108971.g009

100 ps time period. Final MD was carried out for 3000 ps (3 ns) under Particle Mesh Ewald (PME), electrostatics in NPT condition [53].

Protein Protein Docking and complex simulation

It would be interesting to investigate whether Nbp35 and Cfd1 interact to each other and form complex in *E. histolytica*. Protein docking between Nbp35 and Cfd1 was done using PatchDock server (http://bioinfo3d.cs.tau.ac.il/PatchDock/) [54] with default settings. This server is widely used for the protein-protein docking studies [54–56] and its algorithm based on rigid docking with surface flexibility addressed by intermolecular penetration. PatchDock calculation resulted in three-dimensional transformations of the protein's Cartesian coordinate, which were further refined and scored based on protein-protein interaction energy using Fire Dock algorithm. Complex structure with the lowest interaction energy was taken as the final model for further analysis. Molecular dynamics simulations of Nbp35-Cfd1 complex was performed using the GROMACS 4.0.3 under gromos43a1 force field. The whole simulation experiment was done for 10 ns with 36527 water molecules and 1 Na^+ ion. The same methodology was adopted for simulation of this complex as done in the MD of individual proteins Nbp35 and Cfd1.

Co-purification by affinity chromatography

In vitro interaction between recombinant Nbp35 and Cfd1 proteins was investigated by co-elution from an affinity column [57]. The bacterial cell pellet overexpressing recombinant Nbp35 protein was dissolved in 10 ml lysis buffer (50 mM Tris-HCl, pH 8.0, 300 mM NaCl, 0.1% triton X-100) supplemented with 1.0 mM PMSF, 1 X protease inhibitor cocktail (100 µl) and 100 µg/ml lysozyme, and incubated at 30°C for 45 mins. The cell suspension was sonicated on ice and lysate centrifuged at 13000 rpm for 20 min at 4°C. The supernatant containing Nbp35 with N-terminal His-tag was loaded onto a Ni^{2+}–NTA column and washed with buffer A (50 mM Tris–HCl, pH 8.0, 300 mM NaCl, 0.1% Triton X 100) containing 10–50 mM imidazole to remove unbound proteins. Purified recombinant Cfd1 protein was digested with thrombin to remove N-terminal-His-tag and eluted from column followed by desalting as described earlier [24]. The digested Cfd1 protein was loaded on the Nbp35 bound Ni^{2+}–NTA column and incubated for 1.0 hr at RT followed by washing with 15 ml each of buffer A containing 10–60 mM imidazole. Finally, column-bound proteins complex was eluted with buffer A containing 200 and 500 mM of imidazole. Eluate proteins complex was analyzed by 10% SDS–PAGE and western blotting [48] with anti-His (1:2000 Santa cruz), anti-Nbp35 (1:2000), and anti-Cfd1 (1:2000) antibodies raised in rabbit as described previously.

Interaction between recombinant protein and amoebic cell lysate

The bacterial cell pellet over-expressing recombinant Nbp35 protein was processed to obtain Nbp35 bound to Ni^{2+}-NTA column as described in the above section. Amoebic cell lysate ($\sim 5 \times 10^7$ cells) was mixed with Ni^{2+}-NTA matrix bound Nbp35 in column and incubated for 1 hr at 25°C for complex formation. The column was washed rigorously with buffer A containing 10–50 mM imidazole to remove the unbound amoebic proteins and bound proteins complex was eluted with buffer A containing 200 & 500 mM imidazole. All the fractions were electrophoresed in 12% SDS-PAGE and transferred to nitrocellulose membrane. The blots were probed with different antibodies; Anti-His (Santa cruz) mouse monoclonal antibody, anti-Nbp35 & anti-Cfd1 antibodies raised in rabbit at 1:2000 dilution. The alkaline phosphatase conjugated anti-rabbit secondary antibody or anti mouse were also used at 1:2000 dilution and finally blots were developed by adding BCIP/NBT solution as per manufacturer's instruction.

Interaction study by immunoprecipitation

The immunoprecipitation experiments were performed using standard protocol [48] with minor modifications. The anti-Cfd1 or anti-Nbp35 antibody (10 µl) was incubated with protein A sepharose beads (100 µl) overnight at 4°C. The beads suspension was centrifuged at 500×g for 2 mins at 4°C, supernatant discarded and pellet fraction washed twice with 1.0 ml PBS. Amoebic cell lysate ($\sim 5 \times 10^7$ cells) was then mixed with antibody bound protein A sepharose matrix in a 1.5 ml tube with gentle mixing of the sample on a suitable shaker and incubated for 90 mins at RT or overnight at 4°C. The mixture was centrifuged at 500×g for 2 mins at 4°C, supernatant discarded and matrix washed twice with 1 ml PBS to remove loosely bound proteins. The bound complex was eluted from beads by boiling in 100 µl of 1× SDS-loading dye for 10 mins at 95°C. Finally, immunoprecipitated complex (I.P.) was collected by centrifugation at 13000 rpm for 30 sec at RT and supernatant applied on 12% SDS-PAGE and transferred to nitrocellulose membrane. The blots were probed with different antibodies as described above & developed by BCIP/NBT solution [48].

Results and Discussion

Modelling of Nbp35 protein

BLASTP search against Protein Data Bank (PDB) using Nbp35 as query sequence did not give any suitable template. The crystal structure of nucleotide-binding protein from *Archaeoglobus fulgidus* (PDB ID: 2PH1_A) shared only 36% sequence identity and 70% query coverage. Large portion of the target sequence remained unaligned which suggested that not so many nucleotide-binding protein structures have been experimentally resolved to date. Five model of Nbp35 were generated using the I-TASSER algorithm which directly modelled the aligned regions from the template structures (2ph1_A &3vx3_A) and the unaligned regions modelled with ab-initio simulations. These models of Nbp35 were generated with C-scores ranging from −1.99 to −3.04. The C-

score is a confidence score and ranges from −5 to 2, with higher scores representing higher confidence in the model [49]. Best three models were selected (M1, M2 and M3) based on their C-scores (−1.99, −2.65 and −2.84, respectively). Discrete optimized protein energy (DOPE) suggested that the second model (M2) revealed the lowest energy (−33600.3349) whereas the other two models DOPE score, i.e., M1 and M3 revealed −33217.539063 and −32761.363281, respectively. The Φ/Ψ distribution of the backbone conformational angle for each residue of the selected structures was calculated. The M1 model revealed the highest 96.7% residues in the most favoured region and additional allowed region. 2.2% residues were found in generously allowed region whereas only 1.1% residues (Leu232, Thr274 and His275) fell in disallowed region. Based on the DOPE score and the Ramachandran plot, the M2 model was considered to be a reliable model used for rest of the study. After loop refinement, final structure with the lowest energy was checked by Profile-3D (DS 2.5). The self-compatibility score for this protein is 133.09 which is much higher than the Verify expected lowest score (68.24) and very close to the Verify expected high score (151.65). Validation of the modelled protein with ProSA-web revealed that the Z score (−6.74) is within the range of native conformations of the crystal structures. The plot showed the energy remains negative for almost all amino acid residues indicating the acceptability of the predicted model. The Verify-3D result of the model showed that 98.80% amino acids had an average 3D-1D score, and thus indicated the reliability of the proposed model. The monomeric Nbp35 is an α/β type protein containing P-loop nucleoside triphosphate hydrolase type domain (70–314). The modelled structure composed of 12 α-helices (α_1-α_{12}) and four-stranded parallel β-sheets (β_1, β_2, β_4, β_5) with one anti-parallel β-sheet (β_3). One β/α/β motif ($\beta_1/\alpha_4/\beta_2$) is present in between two α-helices (α_2 and α_5). ATPase-like, ParA/MinD signature motif (191–272) is formed by a central α-helix (α_8) joined with a β-sheet (β_5) and α-helix (α_9) on either side.

Modelling of Cfd1 protein

In order to proceed for an accurate search of interacting residues of Cfd1, it is indeed necessary to have a robust 3D model of the protein structure. BLASTp search against PDB database did not return any suitable template. Five model were generated (2ph1_A & 3vx3_A as template) using I-TASSER web server with C-score ranging from −1.61 to −3.52. The fourth loop refined model (C-score = −3.26) revealed the lowest DOPE score (−23306.49) and only three residues; Lys20, Val153 and Asn91 fell in disallowed region. The Ramachandran map of the model revealed 95.2% residues in the most favoured region and additional allowed region. The self-compatibility score for this protein is 87.68, which is much higher than the Verify expected lowest score (55.85). The further precision of the model was checked using the ProSA server, where the Z-score (−6.46) depicts the model to be within the domicile of reported X-ray crystal structures till date. Moreover, the Verify-3D results illustrated the compatibility score of ~84% of amino acid residues which assesses the favourability of residue environments within the folded structure. All these validations suggested the robustness and reliability of the proposed model. The modelled Cfd1 is an α-helices dominated protein (8 α-helices and 2 β-sheets) containing P-loop nucleoside triphosphate hydrolase type domain (21–211). A central α-helix is present in CobQ/CobB/MinD/ParA nucleotide binding domain, joined by one α-helix (α_4) and one 3_{10} helix on either side.

Molecular dynamics simulation of Nbp35 & Cfd1 proteins

The simulated Nbp35 and Cfd1 showed an initial jump in the rmsd at 0 ps time, depicts the initial adjustment of the protein model in the solvent condition corresponding to energy minimization and equilibration steps. MD simulations analysis of Nbp35 showed the root mean squared deviation (RMSD) trajectory rose from 0.0 ps to 2000 ps and then attained final stability, whereas Cfd1 model attained final stability after 2400 ps (Fig. 1). Further analysis suggested that both proteins achieved stable confirmation after simulations. After a precise validation protocol for the projected all-atomic simulated 3D model, the protein complex was processed for MD simulations in the explicit solvent condition. All atoms (RMSD) of the modeled system was checked against the time scale as shown in Fig. 2a, regarding its stability which showed the system attained final stability within average fluctuation of 0.4 nm. We have further analyzed complex stability of Nbp35-Cfd in the presence of hydrogen bonds and found very small fluctuation within the complex as compared to complex with water. The root mean square fluctuations (RMSF) plot for the model system depicts the same stability feature (Fig. 2b) and is well correlated with the RMSD plot. Interestingly, Cfd1 showed more flexibility for residues in the range of 35–55 and 150–250 residue numbers, whereas Nbp35 showed flexibility for residues in the range of 1–60, 130–155, 260–270, and 310–315 residue numbers. All these flexibility of residues were expected to be engaged in protein-protein interaction (Fig. 2b).

In-silico protein-protein Interaction study

Protein-protein complex model of Nbp35-Cfd1 as obtained from Patchdock was processed for MD simulations with Newton's laws of motion in explicit solvent conditions. Ever since the algorithm so far developed for an accurate prediction of large biomolecular complex using docking methods is limited to steric and electrostatic compatibility between docking partners. The approach which has been adopted in the present study indicates an apparent prediction of interaction between these proteins. The protein complex shows few structural regions that are responsible for making protein-protein complex formation, possible by virtue of Van der Waals interactions. Further analysis showed the amino acids involved in contacts, viz. Phe33-Lys35, Gly131-Val135 and Ile147-Glu151 of Nbp35; Gly5-Val6, Met34-Asp39 and Gly46-Ala52 of Cfd1 (Fig. 3a). The complex simulation seems to have a converged trajectory, which has been plotted for protein amino-acids, backbone atoms and side chain atoms as a function of time (Fig. 2a). The prime objective of adopting molecular modeling is not to access the exact behavior of proteins in complex state over time period but to tract the stochastic motional behavior of both proteins in complex state. The loops involved in making the proteins complex are found to be in contact throughout the simulation. The main driving force, as found in this study, is Van der Waals interactions that are responsible for association of both proteins for execution of corresponding biological functions. On the other hand, the polar interactions are not found to be important for this protein complex. This had been assessed by taking into account of the hydrogen bonds which were formed between the protein atoms in the complex state and remains constant throughout the simulations. Similar results were also found while accessing the number of hydrogen bonds formed by protein atoms (in complex state) with the water molecules, which are also constant throughout the simulations. Thus, these findings strengthen our observations that hydrophobic forces surpass over hydrophilic forces between Nbp35 and Cfd1 proteins (Fig. 4a). Interestingly, when solvent accessible surface areas (SASA) calculated over the recorded trajectory frames from MD

simulations as a function of time, showed a decrease of almost 15–20 $nm.S^2.N^{-1}$ as shown in (Fig. 4b). This observation demonstrates that the globular folding of proteins get more compact, thereby preserving the hydrophobic residues from getting exposed to the solvent in complex state.

The conformational changes of protein complex were also analyzed by MD simulations in terms of Principal components analysis (PCA), where we have taken into consideration of the first eigenvectors, to trace down the movement of macromolecule. Pczdump was used to prepare the average coordinates from simulation and was used to show the projections of eigenvectors. The approach helps us in correlating the related fluctuations of protein atoms with that of the total fluctuation in the course of simulation. Fig. 3b represents a porcupine plot for backbone atoms (represented in green color) and the red spikes represent the directionality regarding the motional behavior. The structural regions those are in contacts at the interface both of the proteins are shown an enclosed box in Fig. 3b. We also analyzed the polar contacts formed between these two proteins, by analyzing the coordinate files at regular interval from MD trajectory, though the numbers of hydrogen bond remains same but the residues participating varies. An overview of the residue pairs that are in contact, had been generated based upon the average structure and is represented by Contact-map in Fig. 5. Thus, the fundamental observation as found from the simulation study, being the hydrophobic forces, i.e. the Van der Waals interaction plays crucial role in making the protein complex stable, even in the explicit solvent conditions.

Expression and purification of recombinant Cfd1 and Nbp35

The *Nbp35* ORF of 1002 nucleotides encodes a 333 amino acids protein with predicted molecular weight ~36 kDa and an iso-electric point (pI) value 6.05. The Nbp35 protein, related to Cfd1 show 49% amino acid identity with yeast Nbp35 protein [30]. Similarly, the *Cfd1* ORF of 822 nucleotides encodes a 273 amino acids protein with predicted molecular weight ~29 kDa and an iso-electric point (pI) value 4.98. Neither the MITOPROT II program nor Signal IP 4.1 Server, which predicts protein localization in cells, and a Kyte-Doolittle hydropathy plot, suggested any possible cellular localization other than cytosolic distribution for Nbp35 and Cfd1 proteins. The recombinant (rNbp35 and rCfd1) proteins were expressed in *E. coli* BL21 (DE3) and purified to homogeneity using Ni^{2+}-NTA affinity chromatography as shown in Fig. 6. It was observed that rCfd1 expression was higher in soluble form and eluted between 100–400 mM imidazole with high protein yield of ~5 mg/ml. The purified rCfd1 protein gave a single band of ~29 kDa when examined on SDS-PAGE and immunoblot using anti-Cfd1 antibody in parasite lysates (Fig. 6a). Similarly, Nbp35 was also expressed and purified to homogeneity using Ni^{2+}-NTA affinity chromatography (Fig. 6b). It revealed an apparently homogeneous band of 38 kDa on 12% SDS-PAGE that correlates well with predicted molecular mass 36 kDa. The purified rNbp35 and rCfd1 proteins concentration determined by Bradford's method was found to be 0.212 mg/ml (rCfd1), 0.187 mg/ml (rNbp35) and were stable at −80°C for more than six months in the presence of 10% glycerol.

Polyclonal antisera against purified rNbp35 & rCfd1 proteins were raised in adult rabbit showed high titre at final bleed (1:16000 dilution). Antibody against either rNbp35 or rCfd1 recognised a specific and single band both in *E. histolytica* lysate proteins and purified recombinant protein suggesting that a single homologue is present in the parasite (Fig. 6a & 6b). By immunoblot analysis of a series of diluted recombinant proteins (data not shown), we roughly estimated that the *E. histolytica* contains a significant amount of Nbp35 & Cfd1, which consists of approximately 0.01–0.02% of the total proteins.

Biochemical properties of Nbp35 and Cfd1 proteins

The ability to coordinate Fe-S cluster and donate cluster to apo target proteins is a conserved feature of members of the ApbC/Nbp35 family. Cfd1 (present in yeast and *E. histolytica)* shares similarities with, and falls into, the subfamily of P-loop ATPases [58,59]. The purified Nbp35 and Cfd1 proteins were colourless which indicates loss of cluster during purification. The UV-visible spectrum of purified Nbp35 did not show pronounced absorbance at ~400 nm as compared to purified Cfd1 which suggests that Nbp35 clusters are more labile in the presence of oxygen. We therefore, reconstituted Fe-S clusters of Npb35 and Cfd1proteins under reduced conditions as described in the material and methods. The reconstituted spectra of Nbp35 (Fig. 7a) and Cfd1 (Fig. 7b) showed a peak around 410 nm which is characteristic of [4Fe-4S] cluster. We also estimated iron and sulphide content of both purified proteins just after purification and found that rNbp35 and rCfd1 holds 200–253 μM & 56–87 μM of iron and 209±06 μM & 78±12 μM sulfide, respectively. Thus, the results suggest that rNbp35 & rCfd1 hold two [4Fe-4S] & one [4Fe-4S] cluster, respectively.

Interestingly, *in vitro* assembly and transfer of Fe-S clusters on these P-loop NTPases did not required nucleotide binding or hydrolysis. However, in yeast, nucleotide binding and hydrolysis are required for Fe binding to Cfd1 and Nbp35 *in vivo* [41]. In yeast (*S. cereviseae*), the C-terminal domains of scNbp35 and scCfd1 proteins are similar. The C-terminal domain of scNbp35 holds a 4Fe-4S cluster. The mutational study on scCfd1 and scNbp35 proteins has shown that two central cysteine residues (CPXC) of the C-terminal motif are crucial for the co-ordination of the labile [4Fe-4S] clusters and the formation of the Cfd1-Nbp35 hetero-tetramer complex formation, and the viability of the yeast cells [40]. Nbp35 has the capacity to bind a ferrodoxin-like [4Fe-4S] cluster at the N-terminus of each monomer and a single [4Fe-4S] cluster bridging a Nbp35 dimer through the conserved CX2C motif near the C-terminus of each monomer [40]. It has been suggested that the N-terminal ferrodoxin-like cluster on Nbp35 is structural and not subject to transfer to downstream targets, while the C-terminal bridged clusters are transferred to target proteins [40]. In addition, previous work had also shown that when co-expressed in *E. coli*, Cfd1 and Nbp35 form a heterotetrameric complex that bound four [4Fe-4S] clusters upon reconstitution *in vitro* [41]. Above all, the functional relevance of the Cfd1 and Nbp35 lies in the ability to assemble and deliver Fe-S clusters in the cytosol [34,41].

In-vitro and *in-vivo* protein-protein interaction study

To prove *in-silico* interaction, we performed co-purification and immunoprecipitation experiments. Co-purification using *E. coli* rNbp35 lysate and thrombin digested rCfd1 was performed as described in materials and methods and immunoblot analysis of different fractions with anti-Nbp35 and anti-Cfd1 antibodies confirmed the presence of the Nbp35-Cfd1 protein complex in the eluate fractions. Anti-Cfd1 probed blot (Fig. 8a, ii) showed a relatively faint band of digested rCfd1 protein in the eluate fractions (lane 7 & 8) which corresponded to thrombin digested rCfd1 in the input and flow through fractions (lane 4 & 5). Notably, no Cfd1 was detected in the final wash fraction (lane 6) indicating complete removal of any unbound/loosely bound Cfd1 protein. The undigested rCfd1 (lane 3) was observed to be slightly higher than digested rCfd1 in other fractions due to thrombin

mediated cleavage of His tag. Similarly, anti-Nbp35 probed blot (Fig. 8a, i) recognised rNbp35 in the eluate fractions (lane 7 & 8) which corresponded to rNbp35 in *E. coli* lysate overexpressing fraction (lane 1) and purified rNbp35 fraction (lane 2). Again, rNbp35 was not detected in either the digested Cfd1 flow through fraction (lane 5) or final wash fraction (lane 6) indicating complete removal of any unbound/loosely bound rNbp35 protein before elution. To further confirm our results, we probed the same fractions with anti-His antibody (Fig. 8a, iii) which recognised undigested rCfd1 (lane 3), purified rNbp35 (lane 2) as well as rNbp35 in the eluate fractions (lanes 7, 8) whereas digested Cfd1 was not detected in the eluate fractions (lane 7, 8). This shows that Cfd1 co-eluted with rNbp35 in the eluate fraction lacked a his-tag and therefore co-elution is solely due to complex formation with rNbp35 (Fig. 8a, ii). Thus, these results indicate that Nbp35 and Cfd1 interact with each other and form a stable complex supporting our *in-silico* analysis.

The *in-vitro* result was further verified under *in-vivo* conditions by pull down assay using purified rNbp35 protein and *E. histolytica* total lysate, as described in materials and methods section. All the fractions were run on 12% SDS-PAGE and immunoblot probed with anti-His, anti-Nbp35 or anti-Cfd1 antibodies. As shown in Fig. 8b, both anti-His (Fig. 8b, upper panel) and anti-Nbp35 antibody (Fig. 8b, middle panel) detected Nbp35 in the pull down eluate fraction as well as the input (lane 1 & 3) and flow through fraction (lane 2 & 4) which shows that rNbp35 overexpressed in *E. coli* binds with Ni^{+2}-NTA agarose and gets eluted in eluate fraction similar to any other conventional his tagged fusion protein. *E. histolytica* cell lysate possesses endogenous Nbp35 and Cfd1 proteins without His-tag. Immunoblot probed with anti-Cfd1 antibody (lower panel) detected a band for co-eluted Cfd1 in the pull down eluate fraction (lane 6) which corresponded to endogenous Cfd1 in the amoebic lysate (lane 3) and amoebic lysate flow through fraction (lane 4). This shows that endogenous Cfd1 in the lysate was retained by Ni^{+2}-NTA bound rNbp35 even after extensive washing and co-eluted with rNbp35. No band was observed in final wash fraction (Fig. 8b, lane 5) which indicates that all unbound/loosely bound proteins were completely washed away. Thus, pull down assay using *E. histolytica* lysate and rNbp35 proteins shows that Cfd1 protein present in *E. histolytica* cell lysate forms a complex with recombinant Nbp35 by physical interaction between these two proteins and hence pulled down.

Finally, immunoprecipitation with either anti-Nbp35 or anti-Cfd1 antibodies was performed to confirm *in-vivo* interaction between these two proteins. Initially, anti-Nbp35 antibody was used to pull down its partner protein from *E. histolytica* lysate and blot probed with anti-Cfd1 antibody. As shown in Fig. 9 (upper panel), Cfd1 protein was detected in the eluate fraction (lane 5). Similarly, Nbp35 protein was detected in the eluate fraction (Fig. 9, lower panel, lane 5) when anti-Cfd1 antibody was used for pull down. The intense band of 55 kDa corresponds to IgG heavy chain of antibody. We have also detected 2 faint bands, one above Nbp35 and one below Cfd1 with anti-Nbp35 antibody but not with anti-Cfd1 antibody which is probably due to cross reactivity of anti-Nbp35 antibody with other proteins. Although at present, we could not rule out the possibility of other interacting proteins. Thus, our results clearly demonstrate that these two *E. histolytica* proteins, Nbp35 and Cfd1, physically interact with each other to form a stable complex *in vivo*. A similar interaction between these two proteins has been previously reported in yeast [40,41] where they work together to transfer preassembled Fe-S clusters on cytosolic apo-Fe-S proteins. Our reconstitution as well as interaction results favours a similar role for Nbp35 and Cfd1 in *E. histolytica* but the presence of NIF system in place of ISC system for Fe-S cluster assembly in this parasite demands further study on this unique model organism as far as Fe-S cluster assembly mechanism is concerned.

Conclusion

In the present study the two proteins Nbp35 and Cfd1 were cloned, expressed and recombinant fusion proteins purified by affinity column chromatography. Our *in-silico* molecular dynamics simulation studies, *in vitro* pull down assay as well as *in vivo* immunoprecipitation results clearly indicate an interaction between Nbp35 and Cfd1 proteins of CIA machinery to form a stable complex. This interaction may be essential initial step for transfer of preassembled Fe-S clusters on Nbp35-Cfd1 complex through Nar1-Cia1 proteins to target apo-proteins in the non-mitosomal compartment of *E. histolytica*. However, CIA and NIF machineries co-exist in the cytoplasm with completely different antecedents but how they crosstalk remains to be elucidated.

Acknowledgments

We thank Dr. Sandipan Ganguly, Laboratory of Molecular Parasitolgy, NICED, Kolkata, India for providing *E. histolytica* culture. We also thank other Ph. D. students Asif Equbal, Shshi, and Kuljeet for their support and discussion. Shadab (DBT-SRF), K. P. Singh (DST INSPIRE SRF-P), & Amir Zaidi (CSIR-SRF) acknowledge the financial assistance in the form of fellowship support from DBT, DST & CSIR, New Delhi, India.

RMRIMS communication No. RMRI/016/Pub/Dated 07/03/2014

Ethics Statement: "N/A"

Author Contributions

Conceived and designed the experiments: SA MRD VA. Performed the experiments: SA MRD RK AZ KPS. Analyzed the data: SA MRD KPS GCS VA. Contributed reagents/materials/analysis tools: AKR PD TN VA. Wrote the paper: SA MRD KPS VA.

References

1. Clark CG, Roger AJ (1995) Direct evidence for secondary loss of mitochondria in *Entamoeba histolytica*. Proc-Natl-Acad-Sci-U-S-A 92: 6518–6521.
2. Tovar J, Fischer A, Clark CG (1999) The mitosome, a novel organelle related to mitochondria in the amitochondrial parasite *Entamoeba histolytica*. Mol Microbiol 32: 1013–1021.
3. Susin SA, Lorenzo HK, Zamzami N, Marzo I, Snow BE, et al. (1999) Molecular characterization of mitochondrial apoptosis-inducing factor. Nature 397: 441–446.
4. Lill R, Kispal G (2000) Maturation of cellular Fe-S proteins: an essential function of mitochondria. Trends Biochem Sci 25: 352–356.
5. Beinert H, Holm RH, Munck E (1997) Iron-sulfur clusters: nature's modular, multipurpose structures. Science 277: 653–659.
6. Lill R, Muhlenhoff U (2005) Iron-sulfur-protein biogenesis in eukaryotes. Trends Biochem Sci 30: 133–141.
7. Lill R, Muhlenhoff U (2008) Maturation of iron-sulfur proteins in eukaryotes: mechanisms, connected processes, and diseases. Annu Rev Biochem 77: 669–700.
8. Lill R, Hoffmann B, Molik S, Pierik AJ, Rietzschel N, et al. (2012) The role of mitochondria in cellular iron-sulfur protein biogenesis and iron metabolism. Biochim Biophys Acta 1823: 1491–1508.
9. Kispal G, Csere P, Prohl C, Lill R (1999) The mitochondrial proteins Atm1p and Nfs1p are essential for biogenesis of cytosolic Fe/S proteins. EMBO J 18: 3981–3989.
10. Muhlenhoff U, Balk J, Richhardt N, Kaiser JT, Sipos K, et al. (2004) Functional characterization of the eukaryotic cysteine desulfurase Nfs1p from *Saccharomyces cerevisiae*. J Biol Chem 279: 36906–36915.
11. Nakai Y, Umeda N, Suzuki T, Nakai M, Hayashi H, et al. (2004) Yeast Nfs1p is involved in thio-modification of both mitochondrial and cytoplasmic tRNAs. J Biol Chem 279: 12363–12368.

12. Lill R (2009) Function and biogenesis of iron-sulphur proteins. Nature 460: 831–838.
13. Balk J, Pilon M (2010) Ancient and essential: the assembly of iron-sulfur clusters in plants. Trends Plant Sci 16: 218–226.
14. Rouault TA (2012) Biogenesis of iron-sulfur clusters in mammalian cells: new insights and relevance to human disease. Dis Model Mech 5: 155–164.
15. Craig EA, Voisine C, Schilke B (1999) Mitochondrial iron metabolism in the yeast *Saccharomyces cerevisiae*. Biol Chem 380: 1167–1173.
16. Muhlenhoff U, Lill R (2000) Biogenesis of iron-sulfur proteins in eukaryotes: a novel task of mitochondria that is inherited from bacteria. Biochim Biophys Acta 1459: 370–382.
17. Tovar J, Leon-Avila G, Sanchez LB, Sutak R, Tachezy J, et al. (2003) Mitochondrial remnant organelles of *Giardia* function in iron-sulphur protein maturation. Nature 426: 172–176.
18. Dolezal P, Smid O, Rada P, Zubacova Z, Bursac D, et al. (2005) *Giardia* mitosomes and trichomonad hydrogenosomes share a common mode of protein targeting. Proc Natl Acad Sci U S A 102: 10924–10929.
19. Tsaousis AD, Ollagnier de Choudens S, Gentekaki E, Long S, Gaston D, et al. (2012) Evolution of Fe/S cluster biogenesis in the anaerobic parasite *Blastocystis*. Proc Natl Acad Sci U S A 109: 10426–10431.
20. Changmai P, Horakova E, Long S, Cernotikova-Stribrna E, McDonald LM, et al. (2013) Both human ferredoxins equally efficiently rescue ferredoxin deficiency in *Trypanosoma brucei*. Mol Microbiol 89: 135–151.
21. Seeber F (2002) Biogenesis of iron-sulphur clusters in amitochondriate and apicomplexan protists. Int J Parasitol 32: 1207–1217.
22. Kumar B, Chaubey S, Shah P, Tanveer A, Charan M, et al. (2011) Interaction between sulphur mobilisation proteins SufB and SufC: evidence for an iron-sulphur cluster biogenesis pathway in the apicoplast of *Plasmodium falciparum*. Int J Parasitol 41: 991–999.
23. Ali V, Nozaki T (2013) Iron-sulphur clusters, their biosynthesis, and biological functions in protozoan parasites. Adv Parasitol 83: 1–92.
24. Ali V, Shigeta Y, Tokumoto U, Takahashi Y, Nozaki T (2004) An Intestinal Parasitic Protist, *Entamoeba histolytica*, Possesses a Non-redundant Nitrogen Fixation-like System for Iron-Sulfur Cluster Assembly under Anaerobic Conditions. J Biol Chem 279: 16863–16874.
25. Gill EE, Diaz-Trivino S, Barbera MJ, Silberman JD, Stechmann A, et al. (2007) Novel mitochondrion-related organelles in the anaerobic amoeba *Mastigamoeba balamuthi*. Mol Microbiol 66: 1306–1320.
26. Nyvltova E, Sutak R, Harant K, Sedinova M, Hrdy I, et al. (2013) NIF-type iron-sulfur cluster assembly system is duplicated and distributed in the mitochondria and cytosol of *Mastigamoeba balamuthi*. Proc Natl Acad Sci U S A 110: 7371–7376.
27. Muller M, Mentel M, van Hellemond JJ, Henze K, Woehle C, et al. (2012) Biochemistry and evolution of anaerobic energy metabolism in eukaryotes. Microbiol Mol Biol Rev 76: 444–495.
28. Sheftel A, Stehling O, Lill R (2010) Iron-sulfur proteins in health and disease. Trends Endocrinol Metab 21: 302–314.
29. Roy A, Solodovnikova N, Nicholson T, Antholine W, Walden WE (2003) A novel eukaryotic factor for cytosolic Fe-S cluster assembly. EMBO J 22: 4826–4835.
30. Hausmann A, Aguilar Netz DJ, Balk J, Pierik AJ, Muhlenhoff U, et al. (2005) The eukaryotic P loop NTPase Nbp35: an essential component of the cytosolic and nuclear iron-sulfur protein assembly machinery. Proc Natl Acad Sci U S A 102: 3266–3271.
31. Balk J, Pierik AJ, Netz DJ, Muhlenhoff U, Lill R (2004) The hydrogenase-like Nar1p is essential for maturation of cytosolic and nuclear iron-sulphur proteins. EMBO J 23: 2105–2115.
32. Balk J, Lobreaux S (2005) Biogenesis of iron-sulfur proteins in plants. Trends Plant Sci 10: 324–331.
33. Zhang Y, Lyver ER, Nakamaru-Ogiso E, Yoon H, Amutha B, et al. (2008) Dre2, a conserved eukaryotic Fe/S cluster protein, functions in cytosolic Fe/S protein biogenesis. Mol Cell Biol 28: 5569–5582.
34. Netz DJ, Stumpfig M, Dore C, Muhlenhoff U, Pierik AJ, et al. (2010) Tah18 transfers electrons to Dre2 in cytosolic iron-sulfur protein biogenesis. Nat Chem Biol 6: 758–765.
35. Van Wietmarschen N, Moradian A, Morin GB, Lansdorp PM, Uringa EJ (2012) The mammalian proteins MMS19, MIP18, and ANT2 are involved in cytoplasmic iron-sulfur cluster protein assembly. J Biol Chem 287: 43351–43358.
36. Stehling O, Vashisht AA, Mascarenhas J, Jonsson ZO, Sharma T, et al. (2012) MMS19 assembles iron-sulfur proteins required for DNA metabolism and genomic integrity. Science 337: 195–199.
37. Gari K, Leon Ortiz AM, Borel V, Flynn H, Skehel JM, et al. MMS19 links cytoplasmic iron-sulfur cluster assembly to DNA metabolism. Science 337: 243–245.
38. Stehling O, Mascarenhas J, Vashisht AA, Sheftel AD, Niggemeyer B, et al. (2013) Human CIA2A-FAM96A and CIA2B-FAM96B integrate iron homeostasis and maturation of different subsets of cytosolic-nuclear iron-sulfur proteins. Cell Metab 18: 187–198.
39. Broderick JB (2007) Assembling iron-sulfur clusters in the cytosol. Nat Chem Biol 3: 243–244.
40. Netz DJ, Pierik AJ, Stumpfig M, Muhlenhoff U, Lill R (2007) The Cfd1-Nbp35 complex acts as a scaffold for iron-sulfur protein assembly in the yeast cytosol. Nat Chem Biol 3: 278–286.
41. Netz DJ, Pierik AJ, Stumpfig M, Bill E, Sharma AK, et al. (2012) A bridging [4Fe-4S] cluster and nucleotide binding are essential for function of the Cfd1-Nbp35 complex as a scaffold in iron-sulfur protein maturation. J Biol Chem 287: 12365–12378.
42. Bych K, Netz DJ, Vigani G, Bill E, Lill R, et al. (2008) The essential cytosolic iron-sulfur protein Nbp35 acts without Cfd1 partner in the green lineage. J Biol Chem 283: 35797–35804.
43. Basu S, Leonard JC, Desai N, Mavridou DA, Tang KH, et al. (2013) Divergence of Erv1-associated mitochondrial import and export pathways in trypanosomes and anaerobic protists. Eukaryot Cell 12: 343–355.
44. Diamond LS, Clark CG, Cunnick CC (1995) YI-S, a casein-free medium for axenic cultivation of *Entamoeba histolytica*, related *Entamoeba*, *Giardia intestinalis* and *Trichomonas vaginalis*. J Eukaryot Microbiol 42: 277–278.
45. Ali V, Hashimoto T, Shigeta Y, Nozaki T (2004) Molecular and biochemical characterization of D-phosphoglycerate dehydrogenase from *Entamoeba histolytica*. A unique enteric protozoan parasite that possesses both phosphorylated and nonphosphorylated serine metabolic pathways. Eur J Biochem 271: 2670–2681.
46. Ali V, Shigeta Y, Nozaki T (2003) Molecular and structural characterization of NADPH-dependent d-glycerate dehydrogenase from the enteric parasitic protist *Entamoeba histolytica*. Biochem J 375: 729–736.
47. Olson JW, Agar JN, Johnson MK, Maier RJ (2000) Characterization of the NifU and NifS Fe-S cluster formation proteins essential for viability in *Helicobacter pylori*. Biochemistry 39: 16213–16219.
48. Sambrook J, Fritsch EF, Maniatis T (2001) Molecular Cloning: a Laboratory Manual, 3nd edn. Cold Spring Harbor: Cold Spring Harbor Laboratory Press, 2001.
49. Roy A, Kucukural A, Zhang Y (2010) I-TASSER: a unified platform for automated protein structure and function prediction. Nat Protoc 5: 725–738.
50. Eswar N, Webb B, Marti-Renom MA, Madhusudhan MS, Eramian D, et al. (2007) Comparative protein structure modeling using MODELLER. Curr Protoc Protein Sci Chapter 2: Unit 2 9.
51. Laskowski RA, MacArthur MW, Moss DS, Thornton JM (1993) "PROCHECK: a program to check the stereochemical quality of protein structures." J Appl Crystallog 26: 283–291.
52. Eramian D, Shen MY, Devos D, Melo F, Sali A, et al. (2006) A composite score for predicting errors in protein structure models. Protein Sci 15: 1653–1666.
53. Ewald PP (1921) "Die Berechnung optischer und elektrostatischer gitterpotentiale." Annals of Physics 369: 253–287.
54. Srinivasan K, Stalin T, Sivakumar K (2012) Spectral and electrochemical study of host-guest inclusion complex between 2,4-dinitrophenol and beta-cyclodextrin. Spectrochim Acta A Mol Biomol Spectrosc 94: 89–100.
55. Sharma A, Nigam A (2010) Structure modeling of novel DNA glycosylase enzyme from oral pathogen *Streptococcus sanguinis*. Bioinformation 5: 136–140.
56. Subramaniam S, Mohmmed A, Gupta D (2009) Molecular modeling studies of the interaction between *Plasmodium falciparum* HslU and HslV subunits. J Biomol Struct Dyn 26: 473–479.
57. Nachin L, Loiseau L, Expert D, Barras F (2003) SufC: an unorthodox cytoplasmic ABC/ATPase required for [Fe-S] biogenesis under oxidative stress. EMBO J 22: 427–437.
58. Dean DR, Bolin JT, Zheng L (1993) Nitrogenase metalloclusters: structures, organization, and synthesis. J Bacteriol 175: 6737–6744.
59. Leipe DD, Wolf YI, Koonin EV, Aravind L (2002) Classification and evolution of P-loop GTPases and related ATPases. J Mol Biol 317: 41–72.

Parasitology International 64 (2015) 24–31

Contents lists available at ScienceDirect

Parasitology International

journal homepage: www.elsevier.com/locate/parint

Immunogenicity and anti-fecundity effect of nanoparticle coated glutathione S-transferase (*Sj*GST) DNA vaccine against murine *Schistosoma japonicum* infection

Evaristus Chibunna Mbanefo [a,b,f], Takashi Kumagai [c], Yukinobu Kodama [d], Tomoaki Kurosaki [d], Rieko Furushima-Shimogawara [c], Mahamoud Sama Cherif [a,b], Shusaku Mizukami [a,b], Mihoko Kikuchi [a,b], Nguyen Tien Huy [b,e], Nobuo Ohta [c], Hitoshi Sasaki [d], Kenji Hirayama [a,b,*]

[a] *Department of Immunogenetics, Institute of Tropical Medicine (NEKKEN) and Global COE Program, Nagasaki University, 1-12-4 Sakamoto, 852-8523, Japan*
[b] *Graduate School of Biomedical Sciences, Nagasaki University, 1-12-4 Sakamoto, 852-8523, Japan*
[c] *Section of Environmental Parasitology, Tokyo Medical and Dental University Graduate School of Medical and Dental Science, 113-8519, Japan*
[d] *Department of Hospital Pharmacy, Nagasaki University Hospital, 1-7-1 Sakamoto, 852-8501, Japan*
[e] *Department of Clinical Product Development, Institute of Tropical Medicine (NEKKEN), Nagasaki University, 1-12-4 Sakamoto, 852-8523, Japan*
[f] *Department of Parasitology and Entomology, Faculty of Bioscience, Nnamdi Azikiwe University, P.M.B. 5025, Awka, Nigeria*

ARTICLE INFO

Article history:
Received 7 October 2014
Received in revised form 10 December 2014
Accepted 11 January 2015
Available online 17 January 2015

Keywords:
Schistosoma japonicum
Glutathione S-transferase (GST)
Anti-fecundity
Nanoparticle
DNA vaccine
Gene delivery

ABSTRACT

There is still urgent need for a vaccine against schistosomiasis, especially in *Schistosoma japonicum* endemic areas where even a vaccine that will interrupt zoonotic transmission will be potentially effective as an intervention tool. We had developed a novel nanoparticle gene delivery system, which has proven efficacious in gene transfection to target immune cells with complementary adjuvant effect and high protective efficacy in several diseases. Here, we applied this nanoparticle system in combination with *S. japonicum* glutathione S-transferase (*Sj*GST) DNA vaccine to show the immunogenicity and anti-fecundity effect of the nanoparticle coated vaccine formulation against murine schistosomiasis. The nanoparticle-coated DNA vaccine formulation induced desired immune responses. In comparison with the nanoparticle coated empty vector, it produced significantly increased antigen-specific humoral response, T-helper 1 polarized cytokine environment, higher proportion of IFN-γ producing $CD4^+$ T-cells and the concomitant decrease in IL-4 producing $CD4^+$ T-cells. Although there was no effect on worm burden, we recorded a marked reduction in tissue egg burden. There was up to 71.3% decrease in tissue egg burden and 55% reduction in the fecundity of female adult worms. Our data showed that *Sj*GST DNA vaccine, delivered using the nanoparticle gene delivery system, produced anti-fecundity effect on female adult schistosomes as previously described by using conventional subunit vaccine with adjuvant, proving this DNA vaccine formulation as a promising candidate for anti-pathology and transmission blocking application.

1. Introduction

Schistosomiasis is still an important helminthic infection in terms of severe morbidity that can result as a consequence of infection. It disproportionately affects people with limited access to potable water and sanitation in the tropics and subtropics, with over 240 million people infected and more than 700 million people at risk of getting infected [1]. Although the disease can be effectively treated with the drug of choice Praziquantel (PZQ), reinfection occurs rapidly after mass drug administration (MDA). An effective vaccine used singly or in combination with chemotherapy is the optimal approach, especially in *Schistosoma japonicum* endemic areas where zoonotic transmission from non-human mammalian reservoirs complicates control efforts [2]. The potential for the emergence of PZQ-resistant parasite progenies underscores the need for a vaccine [3]. While an anti-schistosomiasis vaccine that elicit reduction in worm burden is desirable, anti-fecundity vaccines will be equally effective since the parasite eggs account for both the severe pathogenesis [4–6] and continued transmission [2]. In fact, Bilhvax (*Sh*GST), the most advanced vaccine against urogenital schistosomiasis in phase III clinical trial, induces anti-fecundity targeted immune response against *Schistosoma haematobium* [7,8]. Such anti-fecundity vaccine is urgently needed in *S. japonicum* endemic areas where they could initially be deployed to interrupt zoonotic transmission [9–14].

One of the major challenges in schistosomiasis vaccine development is the identification of antigens that can induce the desired immune responses leading to host resistance to reinfection. Several

* Corresponding author at: Department of Immunogenetics, Institute of Tropical Medicine (NEKKEN), Nagasaki University, 1-12-4 Sakamoto, 852-8523, Japan. Tel.: +81 958197820.
E-mail address: hiraken@nagasaki-u.ac.jp (K. Hirayama).

http://dx.doi.org/10.1016/j.parint.2015.01.005
1383-5769/

human studies in endemic areas have provided insight into the potential resistance inducing immune response for schistosomiasis [2,15–19]. Although this subject is still strongly debated, there is a consensus on the involvement of Th1 type of immune response for induction of protective immunity against human schistosomiasis [16,18], and a correlation between levels of IL-10 and susceptibility to schistosomiasis [16,20]. Indeed, protective immunity elicited by vaccination with radiation-attenuated cercariae and other promising vaccine candidates have shown to be Th1 mediated [21–30]. Co-administration of several vaccine antigens with adjuvants with capacity to potentiate Th1 responses and reduce immunoregulatory responses have also shown improved protective efficacy [28, 31–38]. *S. japonicum* 26 kDa GST which has consistently proved to be one of the most promising candidates against Asian schistosomiasis has been shown to induce mainly Th1 response, leading to high antifecundity effect with very significant reduction in liver and intestinal egg burden, albeit with minimal but significant reduction in worm burden [13,14,28,39,40].

DNA vaccination has distinct advantage over other traditional systems, and is considered safe and amenable for application in disease interventions [41]. However, one of the major challenges of this novel approach is the gene delivery system for the optimum delivery of the vaccines to target cells, and adjuvant for the induction of desired type of immune response [41,42]. To address this, we had developed a number of novel nanoparticle (NP) formulations for optimum gene delivery and induction of desired immune response [43–47]. One of the most promising novel nanoparticles is a ternary complex of plasmid DNA, polyethylenimine (PEI) and gamma polyglutamic acid (γ-PGA) [43]. It is a very efficient gene delivery system which is taken up by the target cells through γ-PGA specific receptor mediated energy-dependent process, with consistently high transfection efficiency and low toxicity to mammalian cells [43]. This nanoparticle gene delivery system has been tested for DNA vaccination against many diseases, with results showing consistently high transfection efficiency and significantly improved vaccine effects [47–50]. Here, we have applied this system for DNA vaccination against murine *S. japonicum* infection using the promising 26 kDa *Sj*GST vaccine candidate. Our results showed induction of mainly Th1 immune response, which significantly reduced the fecundity of the female adult worms, even with limited reduction in worm burden.

2. Materials and methods

2.1. Ethics statement

This study adhered to the recommendations in the Fundamental Guidelines for Proper Conduct of Animal Experiment and Related Activities in Academic Research Institutions under the jurisdiction of the Ministry of Education, Culture, Sports, Science and Technology, Japan (Notice No: 71). All animal experiments were performed according to Japan guidelines for use of experimental animals and approved by the Ethics Committees on Animal Care and Experimentation of Nagasaki University (Approval No: 1307291083-2) and Tokyo Medical and Dental University (Approval No: 0140275A).

2.2. Parasites and experimental animals

Six weeks old female BALB/c mice were purchased from SLC Inc. Labs, Japan. *S. japonicum* (Yamanashi strain) life cycle was maintained using female ICR mice (SLC, Japan) and the snail host *Oncomelania hupensis nosophora* at Tokyo Medical and Dental University, Japan. *S. japonicum* cercariae used for challenge infection were shed from crushed snails following the method we previously detailed [51].

2.3. Construction of S. japonicum glutathione S-transferase plasmid DNA vaccine

The coding sequence of *Sj*GST (GenBank: M14654) was amplified from adult worm cDNA library by PCR using the following pair of primers with *Sal*I and *Bam*HI restriction sites on the forward and reverse primers respectively: Forward-5′-GA***GTCGAC***GTCATGTCCCCT ATACTAGGT-3′ and Reverse-5′-CA***GGATCC***TTATTTTGGAGGATGGTC GCC-3′. The PCR product was directly cloned into the *Sal*I and *Bam*HI restriction sites of the pVR1020 vector (Vical, San Diego, CA) to obtain the pVR1020-*Sj*GST plasmid construct. The plasmid DNA was transformed into Top10′ chemically competent *Escherichia coli* cells (Invitrogen, USA). Ten colonies were picked and analyzed by restriction endonuclease digestion and automated DNA sequencing to identify clones with insert in the correct open reading frame. Large scale DNA vaccine was prepared by amplifying and purifying large amounts of a positive clone using QIAGEN Plasmid Mega kit (QIAGEN, USA), according to manufacturer's instructions. The purified plasmid DNA vaccine was re-suspended in 5% glucose and stored in aliquots at −80 °C until use.

2.4. Nanoparticle (NP)-coated SjGST DNA vaccine formulation

The NP-coated *Sj*GST was prepared by formulation of the ternary complex of plasmid DNA (pVR1020-*Sj*GST), polyethylenimine (PEI) and gamma polyglutamic acid (γ-PGA) as earlier detailed by [43]. Briefly, plasmid DNA (pVR1020-*Sj*GST) solution in 5% glucose (1 mg/mL) and PEI solution (pH 7.4) were mixed by pipetting thoroughly and incubated at room temperature for 15 min. pVR1020-*Sj*GST/PEI complex was then mixed with γ-PGA polyanion by pipetting and again incubated for 15 min at room temperature. The ternary complex (pVR1020-*Sj*GST/PEI/γ-PGA) was constructed at a theoretical charge ratio of 1:8:6 for phosphate of plasmid pDNA:nitrogen of PEI:carboxylate of γ-PGA poly-anion, with 73.4 ± 11.5 nm particle size and −22.8 ± 1.4 mV electric charge (ζ-potential). The size and ζ-potential of the complex were determined using Zetasizer Nano ZS (Malvern Instruments, UK).

2.5. Immunization of mice with nanoparticle-coated DNA vaccine and Challenge infection and assessment of protective efficacy

Six weeks old BALB/c mice (n = 13) were immunized three times biweekly with either 100 μg of the pVR1020-*Sj*GST/PEI/γ-PGA nanoparticle DNA vaccine or pVR1020/PEI/γ-PGA containing NP-coated empty vector, by intra-peritoneal route of administration. Two weeks after the last vaccination, mice were bled from the tail vein to prepare sera for antibody ELISA, and 3–5 mice per groups were sacrificed and spleen aseptically collected for FACS, ELISPOT assay and cytokine analyses.

Two weeks after the last immunization, mice (n = 8–10 per group) were challenged percutaneously with 40 *S. japonicum* (Yamanashi strain) cercariae by abdominal penetration using the cover glass method. Seven (7) weeks post infection; mice were perfused to estimate the worm burden. At the time of perfusion, mice liver and intestines were also collected, weighed and digested overnight in 4% KOH at room temperature with shaking. After washing 3 times with distilled water, the worm burden was determined by microscopy and the tissue egg burden was estimated as a combination of intestinal and liver egg burden. The fecundity was determined by calculating the mean number of egg recovered in tissues per female worm.

2.6. Measurement of antibodies levels by ELISA

IgG and IgG subtype profiles were determined by ELISA using sera collected 2 weeks after last immunization. Briefly, 96-well ELISA plates

(Nunc, Denmark) were coated with 1 μg/ml of *Sj*GST (GenScript, USA) in 100 μl of ELISA coating buffer overnight at 4 °C. After washing four times with PBST, plates were blocked for nonspecific binding using 200 μl/well of PBST containing 0.1% blocking reagent (Roche, Germany) for 2 h at RT, and incubated with 100 μl of 1:200 dilution of sera at RT for 2 h. Plates were then washed four times and incubated with 100 μl of HRP-conjugated goat anti-mouse IgG and IgG subclasses (Southern Biotech, UK), diluted 1:4000 for total IgG and 1:2000 for IgG subtypes for 1 h at RT. After washing five times with PBST, antigen–antibody reactions were detected by adding 100 μl/well of 3,3′,5,5′-tetramethylbenzidine (TMB) substrate (Vector Labs, USA). Color development was stopped after 15 min with 100 μl of 1N H_2SO_4, and the absorbance measured at 450 nm in an automated plate reader (Bio-Rad, USA).

2.7. Analysis of T-cell populations by flow cytometry

Spleens were aseptically removed from each mouse and splenocytes were prepared as detailed by [48]. 1×10^6 splenocytes were dispensed into each FACS tube and the cells were pelleted at 3600 rpm for 90 s and washed once with 2 mL of FACS wash buffer (1× PBS containing 0.02% sodium azide, 1% BSA), and then stained with 3 μl (0.5 μg/μl) Mouse Fcγ-blocking antibody and incubated for 15 min at 4 °C. The cells were washed twice and incubated with a combination of 2 μl each of anti-mouse monoclonal antibodies (anti-CD3-FITC, anti-CD4-APC and anti-CD8-PE) on ice for 30 min in the dark. The stained cells were washed twice and re-suspended in 500 μl of FACS buffer. Data acquisition was performed on BD FACSVerse flow cytometry system and analyzed using the BD FACSuite Application (BD Biosciences, USA).

2.8. Intracellular cytokine staining for quantification of IFN-γ producing T-cells

Intracellular cytokine staining and FACs analysis were performed to quantify the proportions of IFN-γ producing T-cells. The cell surface markers were stained as described in Section 2.7 (anti-CD3 PE). The cells were then fixed/permeabilized using BD Fixation/Permeabilization solution for 30 min at 4 °C. The cells were then washed twice using 1× BD Perm/Wash buffer. The fixed/permeabilized cells were then stained for 30 min at 4 °C in the dark using FITC-conjugated anti-IFN-γ antibody. Appropriate isotype antibody was also included for FACs analysis. The cells were washed twice and resuspended in 500 μl Perm/Wash buffer for FACs acquisition. Data acquisition was again performed on BD FACSVerse flow cytometry system and analyzed using the BD FACSuite Application (BD Biosciences, USA).

2.9. ELISPOT assay for quantification of IFN-γ and IL-4 producing cells

ELISPOT assays to determine the proportions of IFN-γ and IL-4 producing cells in cultured splenocytes stimulated with *S. japonicum* adult worm antigen preparation (SWAP), were performed in duplicates using the mouse IFN-γ ELISPOT and IL-4 ELISPOT kits, respectively (Mabtech AB, Sweden) following manufacturer's instructions and as detailed by [48].

2.10. Cytokine analysis

We measured the levels of a panel of cytokines (IFN-γ, IL-12p40, IL-4, IL-10, TNF-α) in the sera and culture supernatants of splenocytes stimulated with SWAP using Procarta Immunoassay Mouse Multiplex polystyrene beads kit (Affymetrix Inc., USA) in triplicates, according to the manufacturer's instructions. Data acquisition was performed on the LABScan100 Luminex instrument (Luminex Corporation, USA).

2.11. Statistics

Data analysis was performed on GraphPad Prism, v5.00. Student *t*-test was used for normally distributed data; otherwise Mann Whitney test was used to compare differences between two groups. All plotted data are medians with error bars representing interquartile ranges. Statistical significance was designated as $p < 0.05$.

3. Results

3.1. Anti-fecundity effect of nanoparticle (NP)-coated pVR1020-SjGST DNA vaccine

To assess the protective efficacy of NP-coated *Sj*GST DNA vaccine, mice were immunized three times at two week intervals with either NP-coated pVR1020-*Sj*GST or NP-coated pVR1020-Blank DNA vaccines. Protective efficacy of the vaccination was measured by the reduction in worm burden, tissue egg burden and fecundity of the female worms. Although there was no reduction in the adult worm burden, there was reduced proportion of paired worms in mice immunized with NP-coated pVR1020-*Sj*GST vaccine. The tissue egg burden was significantly reduced by up to 71.3% in the group of mice immunized with NP-coated pVR1020-*Sj*GST as compared with the NP-coated blank vector control group (Table 1), with the concomitant reduction in liver pathogenesis (Fig. S1). Also, the female worm fecundity, which was defined as the mean number of egg recovered in tissues per female adult worm, was significantly reduced in the mice immunized with NP-coated pVR1020-*Sj*GST by up to 55% as compared with the control group vaccinated with NP-coated blank plasmid (Table 1). The second trial did not produce same level of reduction in tissue egg burden but the observed anti-fecundity effect was statistically significant in both trials. These results indicate that the NP-coated pVR1020-*Sj*GST DNA vaccination has significant anti-fecundity effect against murine *S. japonicum* infection.

3.2. Humoral immune response induced by nanoparticle-coated pVR1020-SjGST DNA vaccine

To assess antigen specific anti-*Sj*GST antibodies production, we measured the levels of IgG and IgG subtypes in immunized mice sera using recombinant *Sj*GST as antigen. As shown in Fig. 1A, there was highly significant increase in levels of total IgG ($p = 0.0002$) and IgG subtypes: IgG1 ($p = 0.0003$); IgG2a ($p = 0.0005$) and IgG2b ($p = 0.0011$) in mice immunized with NP-coated pVR1020-*Sj*GST as compared with mice immunized with NP-coated pVR1020-Blank plasmid. When SWA was used as antigen in ELISA, similar results were obtained, except that IgG2a was only statistically significant in ELISA with recombinant *Sj*GST (Fig. 1B). These results indicate efficient transfection and production of *Sj*GST specific antibodies in mice immunized with NP-coated pVR1020-*Sj*GST.

3.3. Nanoparticle-coated pVR1020-SjGST DNA vaccine elicits T-helper 1 (Th1) biased cellular immune response

To assess cellular immune responses induced by vaccination with NP-coated pVR1020-*Sj*GST DNA vaccine, we compared the proportions of different T-cell populations in the splenocytes and the effector status of T-helper (Th) cells by flow cytometry and ELISPOT assays. There was no significant difference in the proportions of $CD4^+$ (Fig. 2A) and $CD8^+$ (Fig. 2B) T-cells. In ELISPOT assay using splenocytes from the two groups of mice stimulated with SWA, the proportions of IFN-γ producing Th cells were significantly higher in mice immunized with NP-coated pVR1020-*Sj*GST DNA vaccine as compared with the control group immunized with nanoparticle-coated blank plasmid (446.0 ± 2.828 vs 262.5 ± 16.263, $p = 0.0265$) (Fig. 2C). Conversely, the proportion of IL-4 producing Th cells was apparently reduced in mice immunized with NP-coated pVR1020-*Sj*GST DNA vaccine as compared with

Table 1
Anti-fecundity effect of nanoparticle-coated pVR1020-*Sj*GST DNA vaccine.

Groups	Adult worms Mean ± SE (% reduction)	Tissue egg burden Mean ± SE (% reduction) *p*-value	Fecundity Mean ± SE (% reduction) *p*-value
Trial 1			
Blank (n = 10)	18 ± 3.1	$13.79 \times 10^4 \pm 5.3 \times 10^4$	$3.09 \times 10^4 \pm 0.6 \times 10^4$
*Sj*GST (n = 10)	22.2 ± 1.5 (Nil)	$3.96 \times 10^4 \pm 1.8 \times 10^4$ (71.3%) $p = 0.095$	$1.39 \times 10^4 \pm 0.4 \times 10^4$ (55%) $p = 0.041$
Trial 2			
Blank (n = 8)	22.9 ± 1.7	$50.5 \times 10^4 \pm 3.0 \times 10^4$	$5.24 \times 10^4 \pm 0.4 \times 10^4$
*Sj*GST (n = 8)	22.6 ± 2.0 (Nil)	$38.8 \times 10^4 \pm 4.2 \times 10^4$ (23.2%) $p = 0.0399$	$3.79 \times 10^4 \pm 0.2 \times 10^4$ (27.7%) $p = 0.0085$

the NP-coated blank plasmid control group, but the difference was not statistically significant (32.17 ± 26.248 vs 49.83 ± 7.333, $p = 0.0649$) (Fig. 2D). Furthermore, intracellular cytokine staining of T-cells (Fig. 2E) showed significantly higher proportion of IFN-γ producing T cells in the group of mice vaccinated with NP-coated pVR1020-*Sj*GST DNA vaccine as compared to the NP-coated blank vector control group (5.21 ± 0.286 vs 2.96 ± 0.878, $p = 0.0286$). These results indicate a net pro-inflammatory cellular immune response with more IFN-γ producing Th cells and decreased IL-4 producing Th cells, indicating a dominant Th1 immune response with a concomitant decrease in Th2 response as a result of immunization with NP-coated pVR1020-*Sj*GST vaccines.

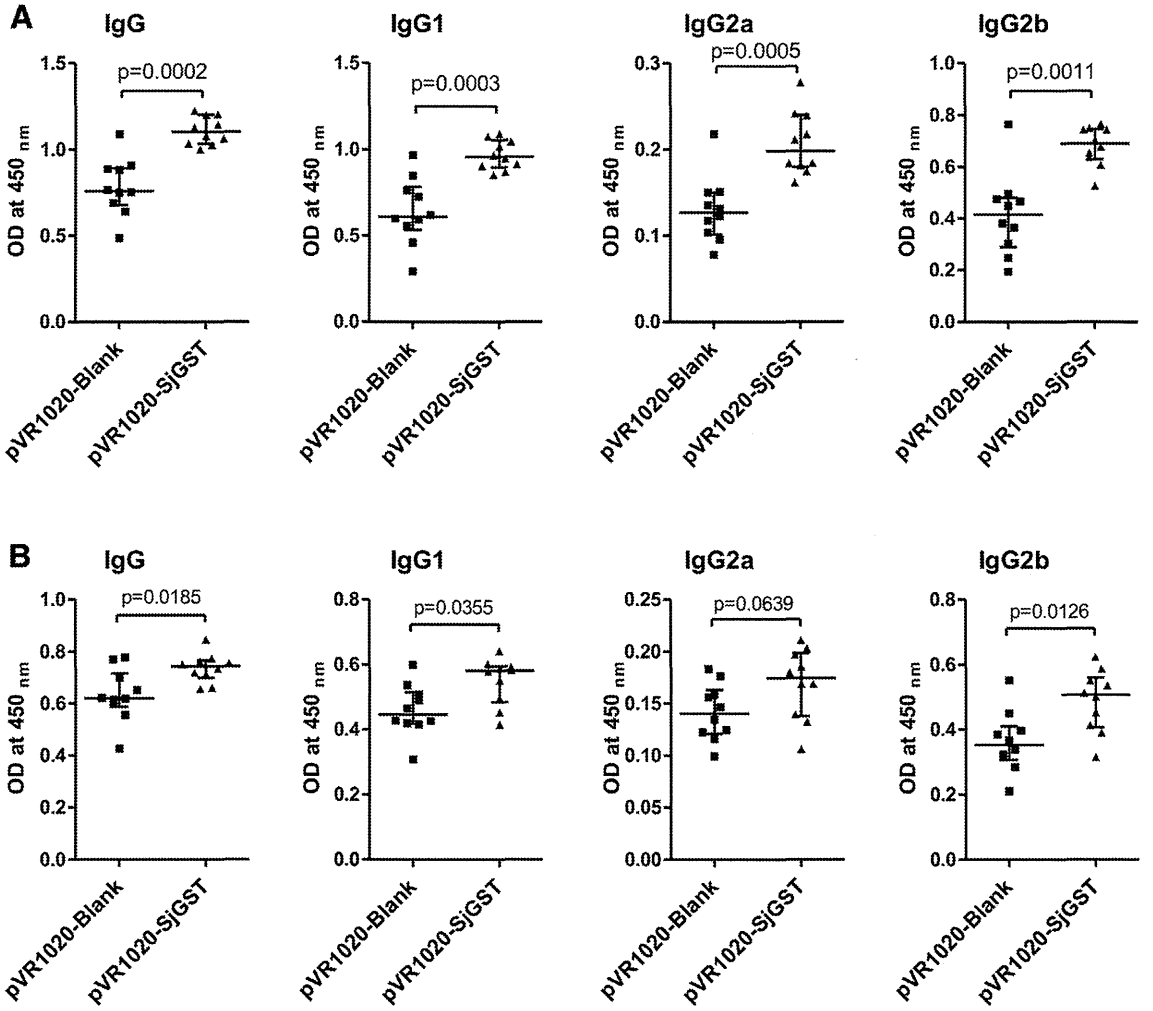

Fig. 1. Humoral immune response induced by nanoparticle-coated *Sj*GST DNA vaccine. (A) *Sj*GST specific total IgG and IgG subtypes were estimated in the sera of mice immunized with either nanoparticle-coated pVR1020-*Sj*GST DNA vaccine or nanoparticle-coated pVR1020-Blank plasmid by ELISA. There was highly significant increase in *Sj*GST-specific IgG and IgG subtypes in the group of mice immunized with nanoparticle-coated pVR1020-*Sj*GST DNA vaccine (n = 10) as compared with the control group (n = 10). (B) When SWA was used as antigen in ELISA, there was still highly significant increase in antibodies levels when compared with both the pre-immune sera and blank plasmid group. The data shown were in triplicates and is a representative of repeated experiments.

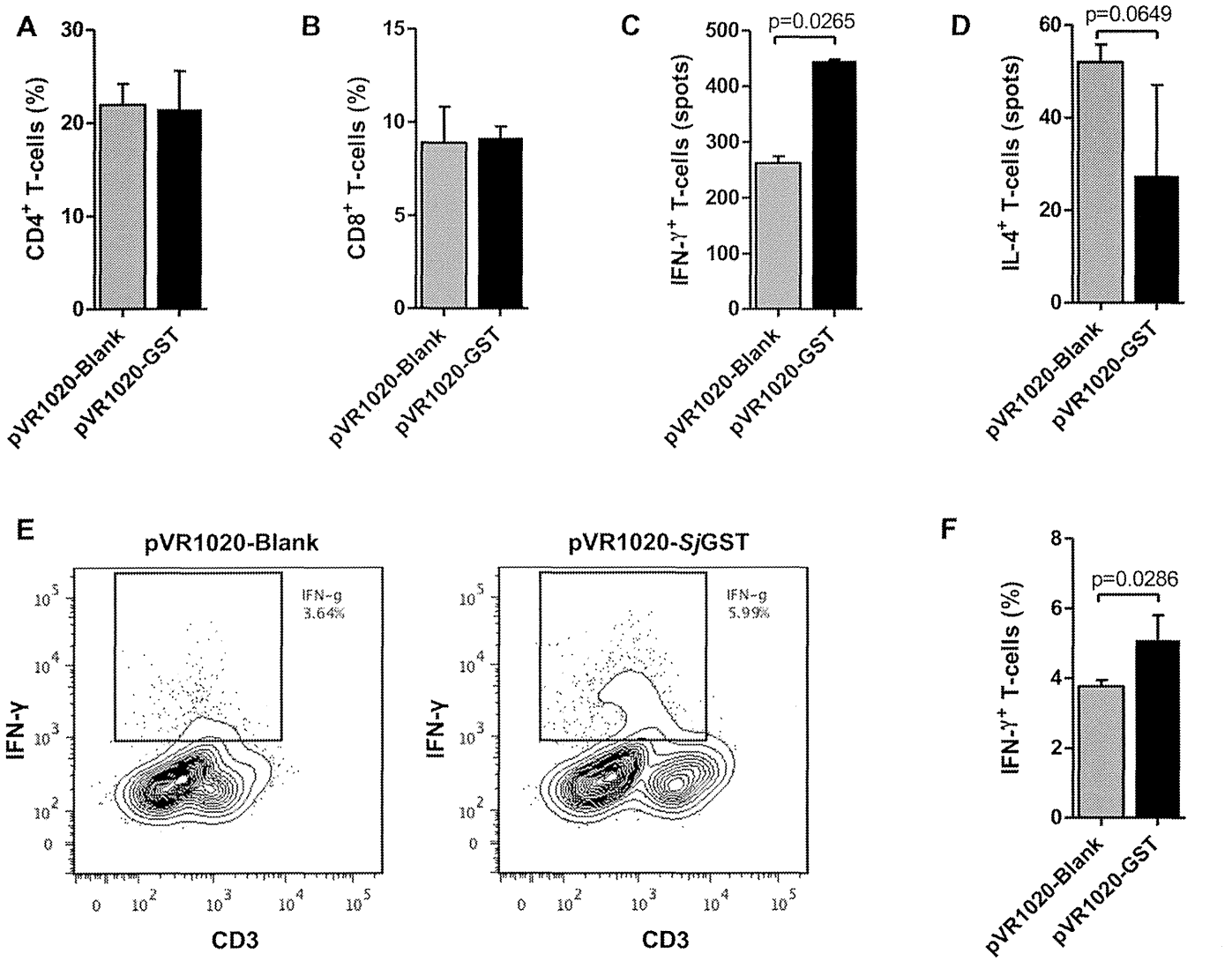

Fig. 2. Nanoparticle-coated *Sj*GST DNA vaccine induces dominant Th1 cellular immune response. Proportions of different T-cell populations in the splenocytes and the effector status of Th cells were evaluated by flow cytometry and ELISPOT assays, respectively. There was no significant difference between the proportions of $CD4^+$ (A) and $CD8^+$ (B) T-cells. The proportions of IFN-γ producing Th cells (C) were significantly higher while the proportion of IL-4 producing Th cells (D) was apparently reduced in mice immunized with nanoparticle-coated pVR1020-*Sj*GST DNA vaccine as compared with the control group immunized with nanoparticle-coated blank plasmid. (E–F) Intracellular cytokine staining showed that there was higher proportion of IFN-γ producing T-cells in mice immunized with nanoparticle-coated pVR1020-*Sj*GST DNA vaccine as compared with the control group. Shown are representative FACs scatter plots (E) and the combined statistics of each group (F).

3.4. Nanoparticle-coated pVR1020-SjGST DNA vaccine induces Th1 cytokine production

To further elucidate the effect of immunization with NP-coated pVR1020-*Sj*GST DNA vaccine, we assessed the levels of a panel of cytokines (IFN-γ, IL-4, IL-12, IL-10 and TNF-α) in the sera (Fig. 3A) and SWA stimulated splenocytes culture supernatants (Fig. 3B) in the two groups of mice. In both sera and splenocyte culture supernatants, there were consistently increased levels of pro-inflammatory and Th1 cytokines in mice immunized with NP-coated pVR1020-*Sj*GST vaccine as compared with mice immunized with the NP-coated pVR1020-Blank plasmid, especially for the serum IL-12 levels which showed statistical significance between the two groups (286.36 ± 75.99 vs 147.42 ± 7.915, $p = 0.035$) (Fig. 3A). Although IL-10 level was reduced in stimulated splenocytes culture supernatant, the difference was not statistically significant. In summary, vaccination with NP-coated pVR1020-*Sj*GST DNA vaccine resulted in the up-regulation of serum IL-12, a pro-inflammatory cytokine which may have driven the Th1 cytokine phenotype of Th cells as shown in Section 3.3 (Fig. 2).

4. Discussion

We have demonstrated significant anti-fecundity effect of nanoparticle-coated *Sj*GST DNA vaccine against murine *S. japonicum* infection. Although a vaccine that will induce sterile protective immunity is more desirable; a vaccine with anti-fecundity effect is equally effective as an anti-pathology and transmission-blocking strategy [2,11]. This is because the host response to egg antigens is responsible for the severe pathogenesis associated with schistosomiasis [4–6]; and the ability of the parasite to pass the eggs with the excreta is the sole means of sustaining disease transmission [2,11,52]. Indeed, Bilhvax (*Sh*GST) which is the most advanced anti-schistosomiasis vaccine candidate in Phase III clinical trial, induces anti-fecundity targeted immune response against *Schistosoma haematobium* [7,8]. Such anti-fecundity vaccines are urgently needed especially in *S. japonicum* endemic areas where zoonotic transmission complicates control efforts [9,10]. However, although zoonosis may represent a major source of reinfection after mass chemotherapy; transmission-blocking interventions targeting zoonotic transmission has been identified as one of the most potent

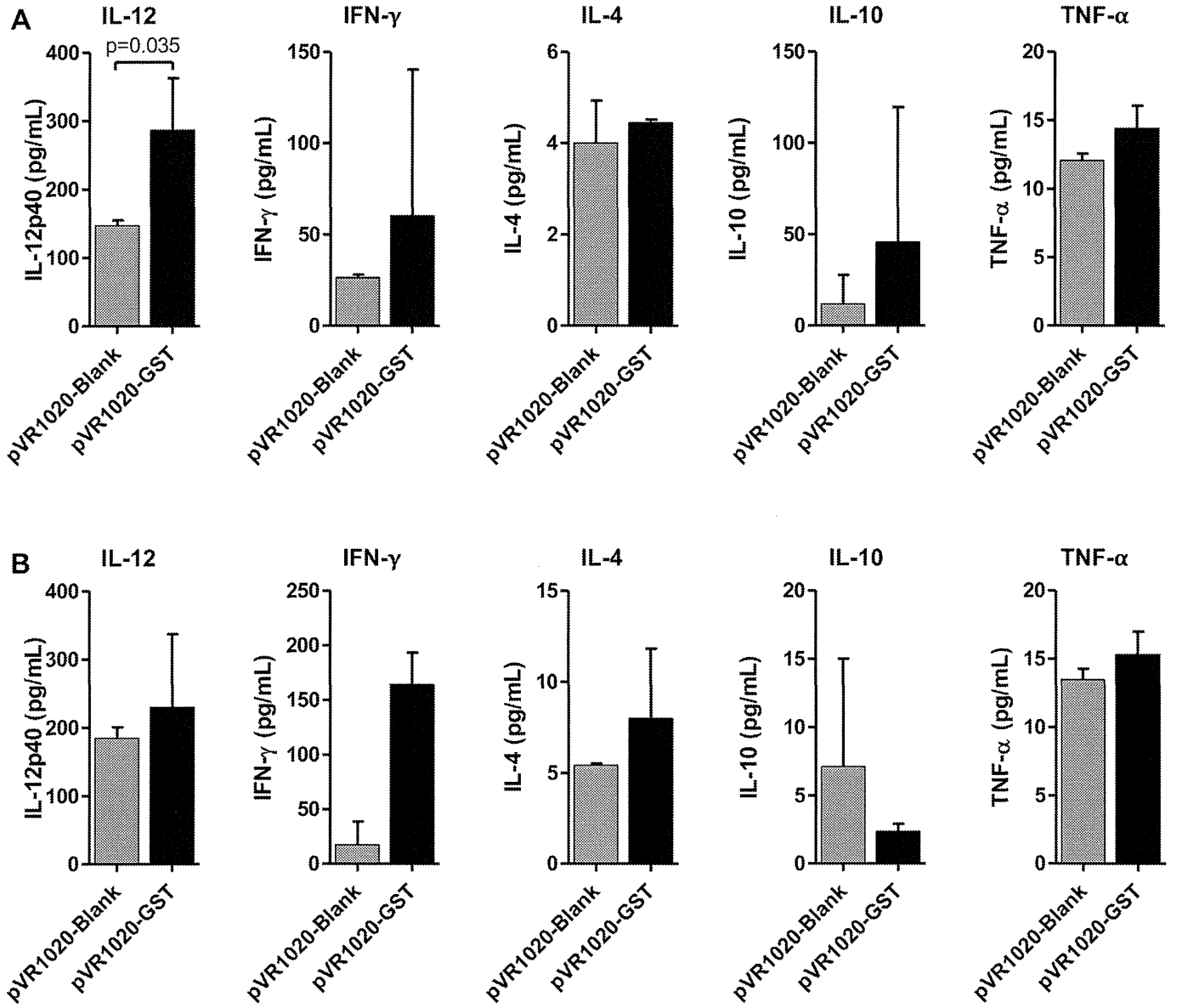

Fig. 3. Nanoparticle-coated *Sj*GST DNA vaccine increases Th1 cytokine production. The levels of a panel of cytokines (IFN-γ, IL-4, IL-12, IL-10 and TNF-α) were estimated in the sera (A) and splenocytes culture supernatants (B) by multiplex cytokine assay. In both sera (A) and splenocytes culture supernatants (B), there was consistently increased levels of pro-inflammatory Th1 cytokines (IL-12, IFN-γ and TNF-α) in mice immunized with nanoparticle coated pVR1020-*Sj*GST vaccine as compared with mice immunized with the nanoparticle coated pVR1020-Blank plasmid. These differences were only statistically significant for serum levels of IL-12 ($p = 0.035$).

strategies for eliminating schistosomiasis in *S. japonicum* endemic areas [2,11]. This is because such vaccine could be initially deployed to interrupt transmission among and from non-human mammalian reservoir hosts [9–14].

DNA vaccination is a promising vaccine strategy [41]. However, for DNA vaccine to effectively induce desired immune response, it is imperative to utilize an effective gene delivery system for optimum transfection of the vaccines to the target immune cells [41,42]. This novel nanoparticle formulation has proven efficacious and has already been deployed for DNA vaccination against many diseases, with results showing consistently high transfection efficiency and significantly improved vaccine effects [47–50]. For the first time, this gene delivery system has been applied for DNA vaccination against a neglected tropical disease, *S. japonicum*; using the promising 26 kDa *Sj*GST vaccine candidate. Our results showed significant anti-pathology and anti-fecundity effect against murine schistosomiasis, as evident in the observed over 71% reduction in tissue egg burden [13,14]. The absence of decrease in worm burden is not unexpected as we had used BALB/c mice; known low responders to *Sj*GST [53]. The choice of this strain was to ensure that any observed protection was not a function of natural resistance by the murine host. However, a marked effect on worm maturation and reduced proportion of paired worms was notable in the *Sj*GST vaccinated mice.

The combination of the nanoparticle gene delivery system and *Sj*GST was very immunogenic, inducing higher levels of antibodies and a dominant Th1 type of immune response as compared to the nanoparticle coated blank vector. Several workers have identified that the presence of polarizing cytokines environment at the time of initial CD4 T-cell activation is the determining factor influencing Th phenotype [54,55]. This vaccine formulation preferentially induced Th1 type of immune response by inducing IL-12 and IFN-γ production. By a characteristic feedback mechanism, persistent exposure to the antigens by an effective gene delivery system activates macrophages by the classical activation pathway to produce more IL-12, which in turn further drives Th1 type of immune response [22,56,57]. Such dominant Th1 type of immune response is arguably required for protective

immunity against human schistosomiasis [16,18]; and sustenance of this Th1 skewed response till the onset of egg production when immune response in schistosomiasis becomes Th2 polarized is correlated with reduced liver egg burden [22,24,58], and is thought to be a potential regulator of egg induced pathology [35]. Indeed, protective immunity elicited by vaccination with radiation-attenuated cercariae and other promising vaccine candidates have consistently proved to be Th1 mediated [21–30,33,34].

The role of host immune response on parasite development is still equivocal, but several studies have recognized that the immunomodulatory shift from Th1 to Th2 is required for normal parasite development, sexual maturation, pairing and reproduction [59–63]. Comparing parasite development in immune-deficient SCID and T-cell deficient nude mice models, Tang et al. (2013) showed that B-cells which are dependent on Th2, promote parasite development, sexual maturation and reproduction [59]. Another study also found that in the absence of IL-7 which is a B-cell growth stimulator; a dominant Th1 response develops, leading to impaired parasite growth and reproduction [63]. Although we have not recorded reduction in worm burden likely due to the mouse strain used, the NP-coated *Sj*GST DNA vaccine formulation induced a Th1 biased immune response. We hypothesize that this Th1 environment has the capacity to prevent the characteristic Th1 to Th2 shift that is required for parasite development; thereby resulting in the observed high proportion of immature worms and low proportion of sexually mature females and paired worms. Indeed, the suppression of parasite induced Th2 switch, which is required for maturation and reproduction, may well represent an effective vaccine mechanism as we showed in this study and as reported by several other workers [21–30,33,34].

In conclusion, we have shown that NP-coated *Sj*GST vaccine showed significant anti-fecundity effect against female adult schistosomes, a relevant characteristic for anti-pathology and transmission blocking application. This vaccine is targeted against zoonotic *S. japonicum*; thus, the vaccine can be initially deployed to interrupt zoonotic transmission from and among non-human mammalian reservoirs in *S. japonicum* endemic areas. Also, the fact that the vector (pVR1020) utilized for this vaccine construct has been adapted and approved for human use [64,65], makes this new strategy highly amenable for translation into a public health product.

Supplementary data to this article can be found online at http://dx.doi.org/10.1016/j.parint.2015.01.005.

Acknowledgments

We are very grateful to Vical Incorporated (Vical, USA) for kindly providing the vector pVR1020 used for the DNA vaccine construct. We thank the members of the Department of Immunogenetics, nstitute of Tropical Medicine, Nagasaki University and Section of Environmental Parasitology, Tokyo Medical and Dental University for useful suggestions and insightful discussions. This study was supported in part by the GCOE Program (2008–2011) and Grant-in-Aid for 21st century COE program (2003–2008), Nagasaki University; and Grant-in-Aid for Scientific Research B and C (22406009 and 23590489) from Japanese Government Ministry of Education, Culture, Science and Technology (MEXT). ECM is a recipient of the Japanese Government MEXT PhD fellowship. The funders had no role in the design, data collection and analysis, manuscript preparation and the decision to publish.

References

[1] King CH. Parasites and poverty: the case of schistosomiasis. Acta Trop 2010;113:95–104.
[2] McManus DP, Bartley PB. A vaccine against Asian schistosomiasis. Parasitol Int 2004;53:163–73.
[3] Cioli D, Pica-Mattoccia L, Basso A, Guidi A. Schistosomiasis control: praziquantel forever? Mol Biochem Parasitol 2014;195:23–9.
[4] Burke ML, Jones MK, Gobert GN, Li YS, Ellis MK, McManus DP. Immunopathogenesis of human schistosomiasis. Parasite Immunol 2009;31:163–76.
[5] Wilson MS, Mentink-Kane MM, Pesce JT, Ramalingam TR, Thompson R, Wynn TA. Immunopathology of schistosomiasis. Immunol Cell Biol 2007;85:148–54.
[6] Andrade ZA. Pathology of human schistosomiasis. Mem Inst Oswaldo Cruz 1987;82(Suppl. 4):17–23.
[7] Capron A, Riveau GJ, Bartley PB, McManus DP. Prospects for a schistosome vaccine. Curr Drug Targets Immune Endocr Metabol Disord 2002;2:281–90.
[8] Beaumier CM, Gillespie PM, Hotez PJ, Bottazzi ME. New vaccines for neglected parasitic diseases and dengue. Transl Res 2013;162:144–55.
[9] Da'dara AA, Li YS, Xiong T, Zhou J, Williams GM, McManus DP, et al. DNA-based vaccines protect against zoonotic schistosomiasis in water buffalo. Vaccine 2008;26:3617–25.
[10] Gray DJ, Williams GM, Li Y, Chen H, Forsyth SJ, Li RS, et al. A cluster-randomised intervention trial against *Schistosoma japonicum* in the Peoples' Republic of China: bovine and human transmission. PLoS One 2009;4:e5900.
[11] McManus DP. Prospects for development of a transmission blocking vaccine against *Schistosoma japonicum*. Parasite Immunol 2005;27:297–308.
[12] Tran MH, Pearson MS, Bethony JM, Smyth DJ, Jones MK, Duke M, et al. Tetraspanins on the surface of *Schistosoma mansoni* are protective antigens against schistosomiasis. Nat Med 2006;12:835–40.
[13] Liu S, Song G, Xu Y, Yang W, McManus DP. Immunization of mice with recombinant Sjc26GST induces a pronounced anti-fecundity effect after experimental infection with Chinese *Schistosoma japonicum*. Vaccine 1995;13:603–7.
[14] Shuxian L, Yongkang H, Guangchen S, Xing-song L, Yuxin X, McManus DP. Anti-fecundity immunity to *Schistosoma japonicum* induced in Chinese water buffaloes (*Bos buffelus*) after vaccination with recombinant 26 kDa glutathione-S-transferase (reSjc26GST). Vet Parasitol 1997;69:39–47.
[15] Figueiredo JP, Oliveira RR, Cardoso LS, Barnes KC, Grant AV, Carvalho EM, et al. Adult worm-specific IgE/IgG4 balance is associated with low infection levels of *Schistosoma mansoni* in an endemic area. Parasite Immunol 2012;34:604–10.
[16] Acosta LP, Waine G, Aligui GD, Tiu WU, Olveda RM, McManus DP. Immune correlate study on human *Schistosoma japonicum* in a well-defined population in Leyte, Philippines: II. Cellular immune responses to *S. japonicum* recombinant and native antigens. Acta Trop 2002;84:137–49.
[17] Jiz M, Friedman JF, Leenstra T, Jarilla B, Pablo A, Langdon G, et al. Immunoglobulin E (IgE) responses to paramyosin predict resistance to reinfection with *Schistosoma japonicum* and are attenuated by IgG4. Infect Immun 2009;77:2051–8.
[18] Brito CF, Caldas IR, Coura Filho P, Correa-Oliveira R, Oliveira SC. CD4+ T cells of schistosomiasis naturally resistant individuals living in an endemic area produce interferon-gamma and tumour necrosis factor-alpha in response to the recombinant 14KDA *Schistosoma mansoni* fatty acid-binding protein. Scand J Immunol 2000;51:595–601.
[19] Mbanefo EC, Huy NT, Wadagni AA, Eneanya CI, Nwaorgu O, Hirayama K. Host Determinants of Reinfection with Schistosomes in Humans: A Systematic Review and Meta-analysis. PLoS Negl Trop Dis 2014;8:e3164.
[20] Wilson MS, Cheever AW, White SD, Thompson RW, Wynn TA. IL-10 blocks the development of resistance to re-infection with *Schistosoma mansoni*. PLoS Pathog 2011;7:e1002171.
[21] Hewitson JP, Hamblin PA, Mountford AP. Immunity induced by the radiation-attenuated schistosome vaccine. Parasite Immunol 2005;27:271–80.
[22] Cardoso FC, Macedo GC, Gava E, Kitten GT, Mati VL, de Melo AL, et al. *Schistosoma mansoni* tegument protein Sm29 is able to induce a Th1-type of immune response and protection against parasite infection. PLoS Negl Trop Dis 2008;2:e308.
[23] He S, Yang L, Lv Z, Hu W, Cao J, Wei J, et al. Molecular and functional characterization of a mortalin-like protein from *Schistosoma japonicum* (SjMLP/hsp70) as a member of the HSP70 family. Parasitol Res 2010;107:955–66.
[24] Zhang Y, Taylor MG, Johansen MV, Bickle QD. Vaccination of mice with a cocktail DNA vaccine induces a Th1-type immune response and partial protection against *Schistosoma japonicum* infection. Vaccine 2001;20:724–30.
[25] Farias LP, Cardoso FC, Miyasato PA, Montoya BO, Tararam CA, Roffato HK, et al. *Schistosoma mansoni* Stomatin like protein-2 is located in the tegument and induces partial protection against challenge infection. PLoS Negl Trop Dis 2010;4:e597.
[26] Ahmad G, Torben W, Zhang W, Wyatt M, Siddiqui AA. Sm-p80-based DNA vaccine formulation induces potent protective immunity against *Schistosoma mansoni*. Parasite Immunol 2009;31:156–61.
[27] Anderson S, Shires VL, Wilson RA, Mountford AP. In the absence of IL-12, the induction of Th1-mediated protective immunity by the attenuated schistosome vaccine is impaired, revealing an alternative pathway with Th2-type characteristics. Eur J Immunol 1998;28:2827–38.
[28] Wang X, Jin H, Du X, Cai C, Yu Y, Zhao G, et al. The protective efficacy against *Schistosoma japonicum* infection by immunization with DNA vaccine and levamisole as adjuvant in mice. Vaccine 2008;26:1832–45.
[29] Zhang R, Yoshida A, Kumagai T, Kawaguchi H, Maruyama H, Suzuki T, et al. Vaccination with calpain induces a Th1-biased protective immune response against *Schistosoma japonicum*. Infect Immun 2001;69:386–91.
[30] Wynn TA, Reynolds A, James S, Cheever AW, Caspar P, Hieny S, et al. IL-12 enhances vaccine-induced immunity to schistosomes by augmenting both humoral and cell-mediated immune responses against the parasite. J Immunol 1996;157:4068–78.
[31] Wang X, Dong L, Ni H, Zhou S, Xu Z, Hoellwarth JS, et al. Combined TLR7/8 and TLR9 ligands potentiate the activity of a *Schistosoma japonicum* DNA vaccine. PLoS Negl Trop Dis 2013;7:e2164.
[32] Fonseca CT, Brito CF, Alves JB, Oliveira SC. IL-12 enhances protective immunity in mice engendered by immunization with recombinant 14 kDa *Schistosoma mansoni* fatty acid-binding protein through an IFN-gamma and TNF-alpha dependent pathway. Vaccine 2004;22:503–10.